DEGREE PROJECT IN ELECTRICAL ENGINEERING,
SECOND CYCLE, 30 CREDITS
STOCKHOLM, SWEDEN 2020

Dielectric Response and Partial Discharge Characteristics of Stator Winding Insulation System with SiC Stress Grading

AMAR ABIDEEN

KTH ROYAL INSTITUTE OF TECHNOLOGY
SCHOOL OF ELECTRICAL ENGINEERING AND COMPUTER SCIENCE

KTH School of Electrical Engineering and Computer Science
Division of Electromagnetic Engineering
SE-100 44 Stockholm
Sweden

ABSTRACT

The typical construction of a stator coil includes the use of end corona protection (ECP) coating, which is made of semi-conductive materials like silicon carbide (SiC). The purpose of ECP is to smooth the electric stress distribution near the slot exit, limiting the electric field and partial discharge (PD) activity within the insulation system. This thesis investigates how ECP affects the dielectric response of a stator coil in high-voltage measurements, both in the time-domain and frequency-domain. It also studies how well time-domain results transformed to the frequency-domain correspond to direct measurements. As a further point, the effect of the ECP on PD activity was demonstrated.

Measurements of dielectric response and PD were made on new coil-halves produced in the usual way in a production run for a motor. The results show that applying the ECP design significantly reduces the PD activity and increases the inception voltage. In addition, the dielectric response of the coil with ECP tape has shown to have a nonlinear voltage dependent characteristic due to the presence of ECP. As the voltage goes higher, this causes a shift of the loss peak toward higher frequency. A distributed-element model of the end section of a stator coil was used to model the nonlinear effect due to ECP, and its results are compared to the measured results. Lastly, FEM simulation of a stator coil end section is presented, showing the contribution of ECP tape in evenly distributing the electric stress near the slot exit.

Keywords: Stator Insulation, Dielectric Frequency Response, Polarization/Depolarization Current, Insulation Modelling, FEM simulation

SAMMANFATTNING

Den typiska konstruktionen av en statorhärva använder ändglimmskydd (ECP), som är tillverkad av halvledande material som kiselkarbid (SiC). Syftet med ECP är att jämna ut det elektriska fältet vid övergången från spåret till ändlindningen, för att undvika högpåkänning och partiell urladdningsaktivitet (PD). Arbetet som presenteras här undersöker hur ECP påverkar den dielektriska responsen hos en statorspole, vid tidsdomän- och frekvensdomänmätningar vid höga spänningar. Den studerar också hur väl tidsdomänresultat som omvandlas till frekvensdomänen motsvarar direkta mätningar. Som en annan punkt visades ECP:s inverkan på PD-aktivitet. Mätningar av dielektrisk respons och PD gjordes på nya statorhärvor som tillverkades för en stor motor. Resultaten visar att tillämpningen av ECP-konstruktionen avsevärt minskar PD-aktiviteten och ökar inceptionsspänningen. Dessutom har spolens dielektriska respons med ECP-tejp visat sig ha en ickelinjär spänningsberoende egenskap på grund av närvaron av ECP. Ökad spänning orsakar en förskjutning av förlusttoppen mot högre frekvens. En modell för ECP användes för att modellera den ickelinjära beteendet, och dess resultat jämförs med mätningarna. Slutligen presenteras FEM-simulering som visar hur ECP gör fältet jämnare.

Keywords: Stator Insulation, Dielectric Frequency Response, Polarization/Depolarization Current, Insulation Modelling, FEM simulation

ACKNOWLEDGEMENTS

First, I would like to express my deepest gratitude to Allah for granting me the strength to continue this work and for blessing me with the world's greatest family, teachers, and friends who were the reason behind accomplishing this work.

My gratitude is extended to my father, mother, sisters, and brother for their continuous support and the constant encouragement to bring out the best of me. Thank you for surrounding me with constant love and support I wish I will be able to show you the same.

A special thanks goes for my employer King Abdulaziz University for granting me this opportunity and for funding my studies. Also, the Cultural Office of the Saudi Embassy for their supervision and support.

My sincere appreciation goes to my supervisor, Jialu Cheng, whom I had the honor and pleasure of sharing many hours in the lab with. With his constant help, I was lucky to have a lifetime opportunity of learning new stuff every day.

My sincere gratitude goes to Nathaniel Taylor, who has provided additional supervision. This work was a complement to some parts of his PhD work. His previous works in stator coil insulation helped me a lot with tackling many issues along the way, in addition to his inputs through my endless emails and meeting.

My appreciation goes to Hans Edin and Patrick Janus for their efforts in the High Voltage course which provided me with the core basics regarding insulation diagnostics.

Special thanks goes to ABB for providing the stator coil samples and Megger for providing the IDAX300 and VAX020, which were necessary for the work accomplishment.

With a special mention to my friends and colleagues: Carmen Dahlin, Emelie Frost, Gustaf André, Max Näf, Simon Lundgren and Stina Carneheim. It was lovely to have the opportunity to work everyday beside you and being part of the Fika crew. Thank you for tolerating my Swedish vowel pronunciation.

LIST OF ABBREVIATIONS

PDC	polarization/depolarization current
DFR	dielectric frequency response
FFT	fast fourier transform
SCP	slot corona protection
ECP	end corona protection
VPI	vacuum pressure impregnation
PD	partial discharge
CvS	curie-von schweidler
PDE	partial differential equation
ODE	ordinal differential equation
HV	high voltage
FEM	finite element method
AC	alternating current
MMF	magnetomotive force
SiC	silicon carbide
IEC	international electrotechnical commission
IEEE	institute of electrical and electronics engineers

LIST OF SYMBOLS

$\sigma(E)$	electric-field dependent conductivity
E	electric field
σ_0	dc conductivity
p	constant used in the empirical model of the electric-field dependent conductivity
E_0	constant used in the empirical model of the electric-field dependent conductivity
C_0	geometric capacitance
A	area
d	distance between two electrodes
ε	effective permittivity
ε_0	permititvity of vacuum
ε_r	relative permittivity
ε_∞	relative permittivity at high frequencies
C_∞	capactiance at high frequencies
χ	electric susceptibility
$P(t)$	time dependent polarization
$D(t)$	time dependent charge displacement
$J(t)$	time dependent current density
U_0	applied dc step voltage
t_c	applied step voltage duration
$i_\mathrm{pol}(t)$	polarization current
$i_\mathrm{depol}(t)$	depolarization current
$\delta(t)$	delta function which is derivative of the step function
$f(t)$	dielectric response function
$\tilde{\chi}(\omega)$	complex dielectric susceptibility
$\chi'(\omega)$	real part of the complex dielectric susceptibility
$\chi'(\omega)$	imaginary part of the complex dielectric susceptibility
$\tilde{\varepsilon}(\omega)$	complex dielectric permittivity
$\varepsilon'(\omega)$	real part of the complex dielectric permittivity
$\varepsilon''(\omega)$	imaginary part of the complex dielectric permittivity
$\tilde{C}(\omega)$	complex capacitance
$C'(\omega)$	real part of the complex capacitance
$C''(\omega)$	imaginary part of the complex capacitance
A_CvS	constant used in curie-von schweidler or fractional-power law universal model of solid insulation materials
$m\ n$	exponent used in curie-von schweidler or fractional-power law universal model of solid insulation materials
A_d	constant used in Debye model of solid insulation materials
τ	time constant used in Debye model of solid insulation materials

k	number of fitted Debye terms
$\tilde{C}_{\text{slot}}$	complex capacitance of stator coil slot section
r	per unit length stress grading tape resistance
c	per unit length capacitance under the stress grading layer
Z_0	characteristic impedance
γ	propagation constant

TABLE OF CONTENTS

LIST OF FIGURES

LIST OF TABLES

CHAPTER I

INTRODUCTION

This chapter briefly introduces why this research is of interest, the aim of the research, and the measurement methods that have been used.

A. Background

In large electric machines, the stator consists of three components: copper conductors, stator core and insulation [1]. The purpose of a typical stator coil insulation system is to prevent any contract between the conductors or the conductor and the grounded core. One of the most common insulation materials is mica. Although mica is known to be PD resistant, poor insulation application can cause the presence of air gaps. Under high electric field stress, these gaps can cause discharges, which can contribute to the degradation of the insulating properties. In severe cases, this can lead to insulation failure, which is known to be one of the significant causes of machine breakdown. A survey done by CIGRE on a total of 1199 hydro generators concluded that 56 % of the breakdown scenes were due to insulation failure [2].

Commonly, the insulation system is made more robust by using two different coatings, which aim to prevent PD on the surface of stator coils or coils. The slot corona protection (SCP) is used in the slot area to avoid any PD caused by air gaps between the coil surface and the stator core. Meanwhile, the end corona protection (ECP) is used near the end of the stator core. The usage of ECP will introduce a nonlinear behavior in the dielectric response of an insulation system.

The dielectric response is known to be a measure that characterizes the dielectric material behavior upon subjected to an electric field. Dielectric response measurement has been commonly used for insulation diagnostic purposes [3]. These measurements can be conducted in the time domain, which is called polarization/depolarization current measurements (PDC) or frequency domain, which is called dielectric frequency response (DFR).

B. Aim

This thesis work is part of a project being carried out by the industrial PhD student Jialu Cheng, supervised by Nathaniel Taylor. Thus, the group involved in this work consisted of Amar Abideen, Nathaniel Taylor and Jialu Cheng. This thesis aims to investigate the influence of nonlinearity of composite insulation on dielectric response and PD activity. Several objectives were listed and act as milestones for the thesis framework, which are:

1) Review the concepts relevant to stator insulation system and its diagnostics.

2) Identify the impact of stress grading materials on PD activity.
3) Identify the impact of stress grading materials on dielectric response through experimental measurements on two stator coil samples, which includes:
   a) DFR/PDC measurements on a stator coil sample without grading material, at different voltages.
   b) DFR/PDC measurements on a stator coil sample with grading material, at different voltages.
4) Investigate the electric stress distribution through FEM simulation of a stator coil sample with grading material at different voltages

C. Method

In this thesis, the following methods were considered to achieve the thesis objective:

1) Literature review of the concepts related to dielectric response measurements and stator insulation system.
2) Design of an experiment to measure the PD of two commercial stator coil sample with and without stress grading material.
3) Design of an experiment to measure the dielectric response of a commercial stator coil sample with and without stress grading material.
4) Perform FEM simulation of a stator coil sample.

D. Publications from this work

A conference paper was prepared and the abstract was accepted to be presented in the 2020 IEEE International Conference on High Voltage Engineering and Application (ICHVE 2020), Beijing, China. The paper is titled "Influence of Nonlinear Stress Grading Material on Dielectric Frequency Response of Stator Insulation". It is based on the experimental part of this thesis.

E. Report structure

The thesis contents are divided into into eight chapters, written to take the reader into a journey from the understanding of a basic stator coil insulation system into measurement/simulation of a commercial stator coil sample. Chapter I was written to shed some light on the thesis motivation, objective and methods. Chapter II was written to familiarize the reader about the basic structure of a typical stator coil insulation system. Chapter III aims to provide the concepts behind using corona protection in stator coils insulation. Chapter IV describes the fundamentals of dielectric response and the differences between a linear and nonlinear insulating material. Chapter V discusses the dielectric response measurements and some Practicalities associated with the measurements. Chapter VI presents the experiment designed to test the stator coil sample along with the results. Chapter VII presents the FEM simulation of a stator coil sample. Finally, the thesis conclusion is presented in Chapter VIII.

CHAPTER II

STATOR COIL INSULATION

This chapter describes the typical construction of a stator coil insulation system.

A. Stator coil design

Electric machines consist of two parts: a part that does not rotate (so-called stationary part or stator) and a part that rotates (so-called rotatory part or rotor). The operation principle of the motor is based on the stator causing a sufficient rotating magnetic field, which causes the rotation of the rotor. In the case of generators, the principle is reversed, i.e. an induced current will flow within the stator windings as a result of the rotating magnetic field from the rotor. However, any machine stator consists of three components: conductors, stator core and insulation [1]. A typical example of the basic construction of a machine stator is shown in Fig. 1 below:

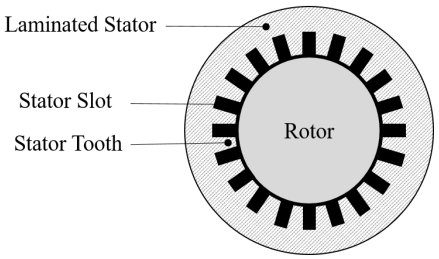

Fig. 1. Basic stator core construction [3]

Electric machines exist in different rated power and voltages. The limitation of raising the voltages comes with the fact that as the machine voltage increases, the electric field stress on the insulation becomes higher. Ideally, the insulation is supposed to prevent any electric current from flowing between the conductor and the insulation surface. However, in practice, there is a slight leakage current flowing through the insulation. This leakage current is further enhanced with the increase of applied electric stress on the insulation. Up to a certain acceptable threshold, the insulation is considered functional. Once the threshold is exceeded, the insulating property is considered lost and the insulation is considered to be electrically conductive. At some severe cases, this can facilitate the creation of a path between the machine conductors and the ground causing a short circuit.

There are several types of stator winding structures: Random-wound stators, Form-wound stators using multiturn coils and Form-wound stators using Roebel bars [1]. The Random-wound stator includes several copper bundles wound through core slots in a concentric formation. This approach is feasible in small machines, typically with a rating of several hundred kW [1]. As the machine size gets larger, form-wound is considered, which involves the distribution of stator windings in several coils [1]. This is done because the conductor insulation would require a thicker layer introducing some mechanical difficulties to have the conductor wound using the conventional way. Form-wound coils are common in most large motors and many generators with ratings up to 50-100 MVA while large generators consider the usage of roebel bar construction [1]. An example of a simple stator coil sketch can be seen in Fig. 2 below:

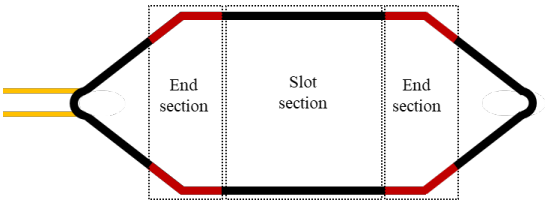

Fig. 2. Example of a multiturn stator coil

The length of the stator coil can be divided into two regions: the slot section and the end section. The slot section of the stator coil is mounted into the core slot. Then, the whole stator would consist of numerous coils symmetrically mounted in slots located on the outer surface of a cylindrical core.

The stationary core is made of magnetic steel since it provides a low-reluctance path for magnetic fields [1]. The cylindrically shaped core consists of several thin steel sheets packed together to form what so-called laminated steel or laminated core. These laminations must be electrically isolated from each other and insulated to prevent the electric field within the machine from inducing substantial eddy currents within the core.

These stator coils can have single or multiple turns. Each turn can include one or several strands. The choice between the number of turns and the number of strands per turn has always been a design problem in which several constraints justify the designer's choice. For example, there is a detailed discussion in [4] about the design considerations of stator coils based on having losses management and harmonic elimination as the main constraints. Finally, a practical example of an assembled motor's stator core can be seen in Fig. 3 below:

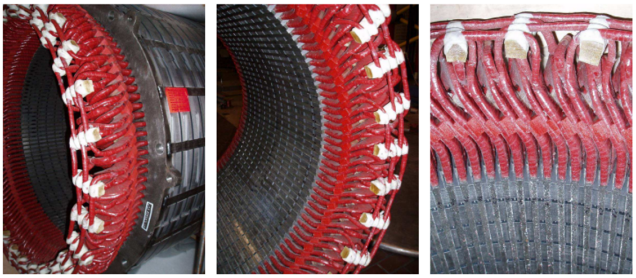

Fig. 3. Example of a motor stator [3]

B. Insulation Construction

Proper insulation system is an essential aspect to consider in the machine design. The insulation system should be designed to ensure that the electrical charges are kept within the conducting layer. This is done by ensuring that the electrical field stress on the insulation will not cause the flow of electrical charges within the insulation medium to exceed the acceptable threshold. In other words, the stator coil insulation system's design is based on investigating the maximum stress points and ensuring that the material has enough breakdown strength to withstand that stress. The conventional insulation system considers the use of the following insulation layers:

1) Strand insulation: The copper strands are insulated with a thin layer of strand insulation, which will have the capacity to withstand around tens of volts per strand [3].
2) Turn insulation: The group of strands forms a single turn, which is insulated by a layer of turn insulation. Turn insulation is expected to withstand hundreds of voltage during the normal operating conditions and have to withstand the transient overvoltages.
3) Main or Groundwall insulation: It is the thickest insulation layer designed to withstand around thousands of volts.

However, in modern stator coils, the strand and the turn insulation layer is considered one and often referred to as conductor insulation. An example of a conventional and modern stator coil insulation is shown in Fig. 4 below:

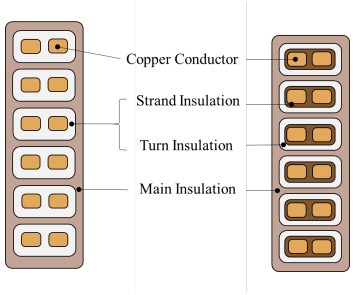

Fig. 4. An example of the old (right) and modern (left) stator coil insulation system

C. Insulation material

The historical development of insulation materials was extensively discussed in [5]. Nowadays, the most common material used as the main insulation in stator coils is mica.

The name mica is used to refer to a group of minerals of silicate that has similar physical properties and related composition. The chemical general formula of micas can be given as [6]:

$$X_2Y_{4\text{-}6}Z_8O_{20}(OH,F)_4$$

where

- X is commonly K, Na, or Ca
- Y is commonly Al, Mg, or Fe
- Z is mainly Si or Al

There are two common types of micas, namely Muscovite and Phlogophite. Some of the notable physical properties of these are shown in Table I below [7]:

TABLE I
ELECTRICAL PROPERTIES OF SOME COMMON MICAS

Properties	**Muscovite**	**Phlogophite**
Dielectric constant	$6-8$	$5-6$
Resistivity [Ω·m]	$10^{15}-10^{16}$	$10^{13}-10^{14}$

The main insulation consists of around 65% mica paper, 25% resin and the glass fabric and other support materials compose 10% [8]. Commonly, the stator coil insulation consists of several layers [9]:

- A barrier made of mica flakes used to prevent partial discharge.
- A support made of glass fiber designed to increase the tensile strength.
- A binder made of epoxy to fill in the gaps between barrier layers.

D. Impregnation of stator coil insulation

The purpose of Vacuum Pressure Impregnation (VPI) is to fill gaps between mica tape layers and small air cavities with resin or other liquids. This process occurs after applying dry mica tapes on the coils then place them on an impregnation chamber. This can be done either by placing each stator coil individually or globally for the whole stator (after the coils on the stator core) [1]. The most basic VPI principle can be illustrated, according to Fig. 5 below:

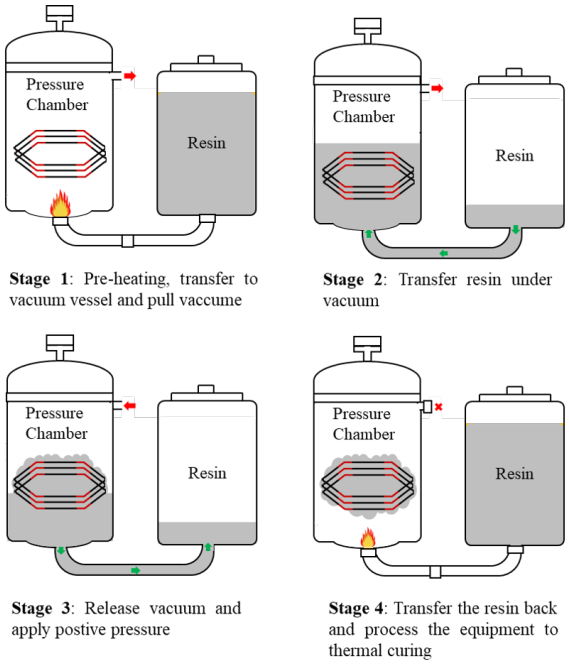

Fig. 5. Summary of VPI processes [10]

The process of VPI starts with the removal of the moistures through pre-heating the chamber and then removing the air from the chamber [11]. Following that, the chamber is filled with resin. Once the objects inside the chamber are submerged in resin, a wet vacuum is created and pressure is applied to ensure that the insulation is impregnated with resin. Moreover, the objects are subjected to thermal curing.

E. Summary

This chapter discussed form-wound coils and stator bars, in contrast to the random-wound stators found at low voltage. The form-wound structure allows using a thicker insulation layer. Modern stator coils design includes conductor stranding and mica based insulation. The manufacturing of modern stator coils starts with using mica tape wrapped around several copper strands. After the application of mica tape, some gaps or small air cavities can be present. Therefore, VPI is considered to fill these gaps with resin or other liquids. The VPI can be done separately for each coil or globally for the whole stator after assembly.

CHAPTER III

CORONA PROTECTION IN STATOR COILS

Generally, the performance of an insulation system can decrease due to degradation caused by partial discharge. The system then has an increased risk of losing the insulation property, which is known as dielectric breakdown. In this chapter, the precautions taken to prevent the stator coil insulation from having corona discharge are discussed.

A. Partial Discharge in stator coils

The International Electrotechnical Commission (IEC) definition of partial discharge is [12]:

> "*Partial discharge (PD) is a localized electrical discharge that only partially bridges the insulation between conductors and which may or may not occur adjacent to a conductor*"

In solid insulation systems, the term 'partial discharge' is used to refer to a group of discharge phenomena which are [13]:

1) Internal discharges occurring in voids or cavities.
2) Surface discharges appearing at the boundary of different insulation materials.
3) Corona discharges occurring in gaseous dielectrics in the presence of inhomogeneous fields.
4) Continuous impact of discharges in solid dielectrics forming discharge channels (electric treeing).

As the insulation materials degrade with time, partial discharge activity is elevated. This impact can even be accelerated or enhanced by the thermal, electrical, ambient, and mechanical stresses that the electric machine is subjected to during its service life. The continuous increase of partial discharge activity can lead to the formation of a so-called electrical tree, which is known to be the pre-breakdown mechanism in solid insulation. As a result, the breakdown threshold of the material starts to fall off. There are many possible factors that could influence the PD in the insulation, e.g. cracks, voids, deterioration, etc.

Although the stator coil's main insulation is made of mica, which has a wide reputation of being PD resistant, the continuous PD can wear the epoxy and mica may be damaged by a strong PD in a cavity that grows. Moreover, the existence of voids or delamination

caused by poor VPI or the degradation can be a potential source of PD. Such voids usually have air molecules that begin to ionize if subjected to a strong electric field (stronger than 3 kV/mm) [14]. An example of insulation defects is shown in Fig. 6 below:

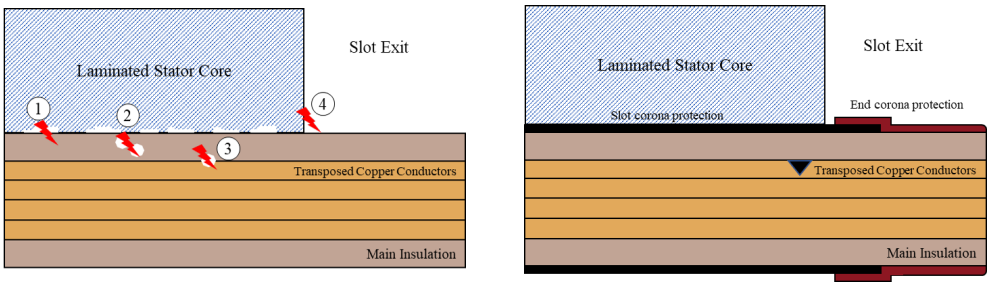

Fig. 6. Cross-section of stator core with insulation defects (left) and corona protection (right) [14]

The points (1-4) indicated in Fig. 6 shows possible PD locations. Voids and delamination within the groundwall insulation (indicated by "2") are related to faulty insulation application, i.e. improper taping or poor VPI [14]. Thus, ensuring an accurate tape application and proper VPI processing can avoid such defects. As for the PD between the main insulation and the copper conductor (indicated by "3"), PD can be avoided by filling the gaps with mastic or using mastic tape. This is referred to as internal corona protection.

Moreover, the external PD or slot discharge (indicated by "1") is the most critical PD location. This is because erosion of the main-wall insulation causes the coil mounted in the slot to loosening up [14]. Then, continuous mechanical vibration will influence the erosion induced by PD. To overcome this, a layer of semiconductive varnish or tape is applied, which has surface resistance[†] from $100\,\Omega$ up to $2\,\mathrm{k}\Omega$ [3].

At the end of the slot exit area (indicated by "4"), the concentration of electric field is high, which can cause surface discharges. To prevent that, *end corona protection* is considered, which is a semiconductive material applied in the form of tape or varnish. This material has a nonlinear voltage/current characteristic and will cause a stress grading effect on the insulation surface. One of the most common materials for used for this purpose is Silicon Carbide (SiC).

B. Electric field distribution around slot exit area

The problem with the stator coil end section comes from the fact that there is a high concentration of electric stress around the slot exit area, which can be sufficient to cause surface discharges. The slot section is covered with a low resistance semi-conductive layer and thus has zero surface potential. As a result, the slot section is not subjected to high electric stress. However, one could propose the idea of extending the slot coating to cover the slot exit area. The problem with this idea is that the electric field concentration in the groundwall insulation at the coating end would increase, causing a potential breakdown of the main insulation. Therefore, the proper solution would be to add another stress grading layer at the end section. Fig. 7 below, demonstrates the difference of field distribution between two designs with and without stress grading layer:

[†]Surface resistance refers to the electrical resistance between two opposite sides of any square slab of the surface [3]. This also used to characterize the resistance of the leakage current path along an insulation surface. The unit used for the surface resistance is Ω or Ω/sq.

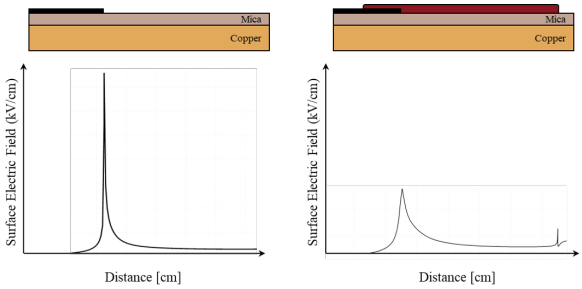

Fig. 7. Electric field distribution at the stator coil end section

It can be concluded, that the ECP is capable of reducing the maximum stress and lead to a better stress distribution compared to the case that ECP is not considered. As a result, the electric field will not be sufficient to cause surface discharg at the end section. The impact of stress grading can be demonstrated through a screenshot of an interesting experiment performed by Quartzelec UK Engineering, which is shown in Fig. 8 below:

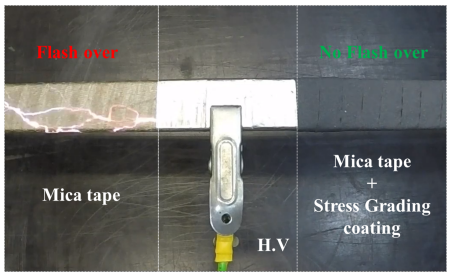

Fig. 8. The impact of stress grading tape [15]

From Fig. 8 above, it can be seen that surface discharge occurs when the insulation system consists of mica tape only. Meanwhile, flashover does not occur when stress grading tape is applied. An important thing to point out here is that there could be small discharges on the section covered with stress coating due to void between the layers of mica tapes. Since this is just an illustration video, the stress graded section might not have been processed using VPI. It is expected that if the end section was treated with proper VPI that these small discharges would not exist since the voids would be filled with resin.

C. Measurements of PD activity in stator coils

The purpose of the PD measurement is to detect the discharge pulses within the tested object. PD measurements can be classified into off-line and on-line measurements. Commonly, the off-line partial discharge measurements are based on applying the test voltage across the main insulation then measuring the current pulses due to PD. The test voltage can be similar to the rated voltage or different, e.g. offline measurements can be done in steps from 40% to 120% of the rated line-line or line-ground voltage. Also, off-line measurements require the object under test to be disconnected, i.e. performed before dispatching or during maintenance of the object under test. Meanwhile, the on-line partial discharge measurements are done during the normal operation of the whole machine [1].Technical standards like IEC 60034-27-1:2017 and IEC TS 60034-27-2:2012 describe how to perform off-line and on-line partial discharge measurements on winding insulation, respectively.

The PD activity measurements in a stator coil will detect a group of discharge pulses following a certain pattern, depending on the type of the discharge. The PD pattern may give some insight about which kind of defect is the insulation system has. An example of some of the commonly seen PD patterns is shown in Fig. 9 below [16], [17], [18]:

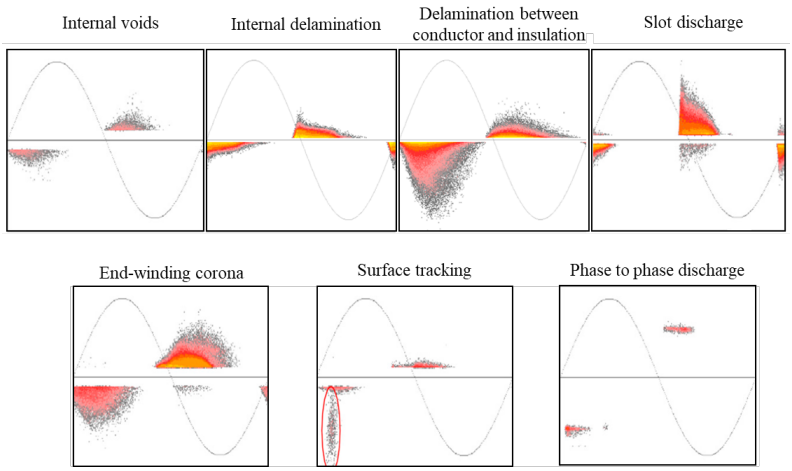

Fig. 9. Common PD pattern in stator coils [18]

The primary concern is to verify that the addition of stress grading tape to an insulation system would eliminate the end winding PD (PD discharges that are not related to any insulation defects). This is achieved through a simple PD measurement of two stator coils produced identically, except that one is normally produced and the other has no ECP tape applied. The detailed design parameters of the stator coils are presented later in Chapter VI. The laboratory setup used for PD measurements is shown in Fig. 10 below:

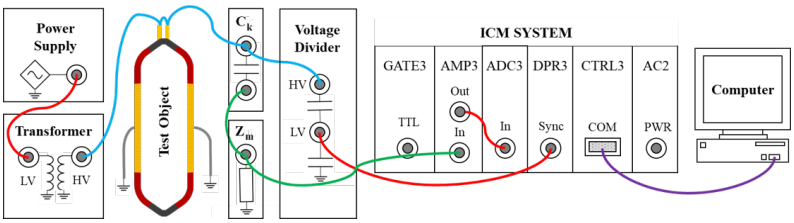

Fig. 10. PD measurement circuit scheme

The power supply is used to control the input voltage fed into the low voltage side of a transformer. The high voltage side of the transformer is connected to three branches. The first branch is connected to the stator coil conductor. Meanwhile, the other two branches include the PD measurement impedance Z_m in series with the coupling capacitor C_k and the voltage divider, respectively. The PD signal and external voltage reference from this setup are fed to the ICM system, which is a PD measurement device. The PD signal is taken from the connection point between the measurement impedance Z_m and the coupling capacitor C_k. This signal is processed through an amplifier module (AMP3), which includes a peak-meter that captures the PD pulses. Then, the signal is fed to an analog to digital converter (ADC3), which will classify the pulses level using a 256 digital levels scale

[3]. The second signal is taken from the voltage divider and fed into the DPR3 module, which serves as a dual-port ram and synchronizer. The basic operation of the PD activity measurement is straight forward. The voltage will be increased slowly until the PD activity is observed. This voltage is known as PD Inception Voltage. The inception voltage and a picture of the PD activity is recorded. This was done on the two stator coil samples where the PD pattern shown in Fig. 11 was obtained:

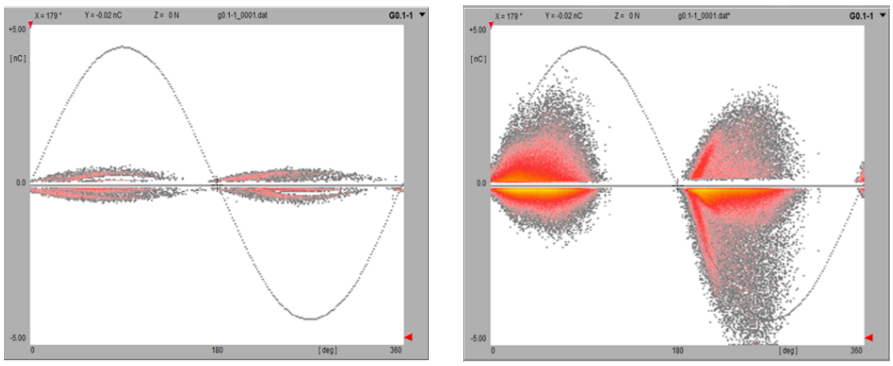

Fig. 11. PD measurement of stator coil with ECP (left) and coil without ECP (right)

The inception voltage was 4.1 kV and 5 kV for the coil with and without ECP tape, respectively. From the pattern shown in Fig. 11, it can be concluded that the PD activity is more severe in the coil sample without ECP. As for the reason of PD, it is not easy to point out the actual source since the obtained PD pattern does not follow any of the specific patterns described earlier in Fig. 9. However, this test was just a verification that the use of ECP would avoid some of the potential PD activity of a coil without ECP.

D. Electrical property of Stress grading material

The stress grading material behaves like an electric-field dependant resistor, which exhibits high resistance when the electric field is low and low resistance when the electric field is high. The basic characteristics of the stress grading material electrical conductivity over the electric field is shown in Fig. 12 below:

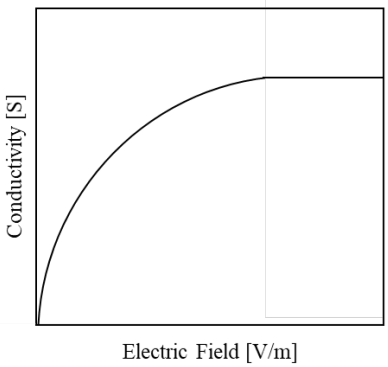

Fig. 12. Basic characteristics of a material with field-dependent conductivity

Silicon Carbide (SiC) exhibits similar characteristics as shown in Fig. 12 above. From several practical measurements on SiC grading tape, it has been empirically found that the field-dependent conductivity can be well fitted by an exponential-of-power expression such as [3]:

$$\sigma(E) = \sigma_0 e^{\left[\frac{|E|}{E_0}\right]^p} \quad \text{[S/m]} \tag{1}$$

where

- σ_0 is the DC conductivity [S/m]
- E_0 is a constant determined by fitting the expression to a set of measured data [V/m]
- E is the electric field [V/m]
- p is a constant determined by fitting the expression to a set of measured data. A majority of literature suggests that, the typical value of the exponent is around 2/3 [3].

SiC has been known to be one of the most favorable materials for stress grading purposes due to its high breakdown electric field strength, high-temperature resilience and commercial availability [19]. This is not a surprise since SiC was previously used in lightning overvoltage protection (lightning or surge arrester) before ZnO. The addition of SiC tape to the insulation system will lead to a high non-linear surface resistance, which can be around a few gigaohms at 300 V/mm. Moreover, the usage of Silicon Carbide (SiC) will cause a non-linear current/voltage-gradient relation.

E. Summary

This chapter described the basic concepts related to corona protection in stator coils. The main problem arises from PD produced at the boundary of main insulation and core as well as slot exit area. The most basic construction involves having a slot corona protection layer and end corona protection layer. The electric field distribution along the slot section can be neglected because it is well below the breakdown strength of main insulation compared to the end section. As demonstrated previously, the use of ECP in the end section helps facilitate a better stress distribution. As a result, the risk of having surface discharges in the end section is lowered. This was verified through PD measurements of two stator coil samples with and without ECP. The coil sample with ECP has shown to be more PD resistant than the other sample. Furthermore, the complete coil insulation system with corona protection can be illustrated, as shown in Fig. 13 below:

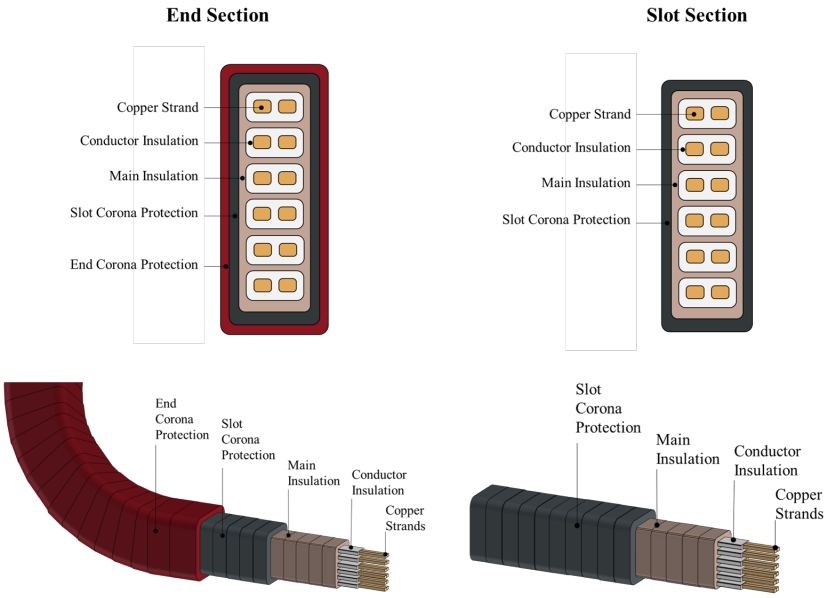

Fig. 13. The construction of stator coil insulation with corona protection

CHAPTER IV

DIELECTRIC RESPONSE

A dielectric material is often known as an electrical insulator, which tends to polarize upon being subjected to an electric field. The dielectric response is the measure of how the material reacts upon being subjected to an electric field. This chapter introduces some basics about the dielectric response of insulation material.

A. Time Domain Polarization of dielectrics

When an electric field is applied across a dielectric material sample, it exerts a force on the dipoles, causing the rotation of dipoles. As a result, a small current flows through the dielectric material. The current magnitude decays over time as the number of dipoles aligned with the external field reaches an equilibrium. In a isotropic dielectric material, the displacement of charges over time is denoted as $D(t)$, which can be given as [13]:

$$D(t) = \varepsilon_0 E(t) + P(t) \tag{2}$$

Fundamentally, the polarization occurs in two different mechanisms: rapid and slow. The time dependent polarization can be expressed as [13]:

$$P(t) = \varepsilon_0 \chi(0) E(t) + \varepsilon_0 \int_0^t E(\tau) \frac{\mathrm{d}\chi(t-\tau)}{\mathrm{d}t} \mathrm{d}\tau \tag{3}$$

In (3) above, ϵ_0 is the permittivity of free space, 8.854×10^{-12} F/m. The degree of how "well" the material polarizes is characterized by a dimensionless parameter called electric susceptibility χ. The derivative of susceptibility χ is the dielectric response function $f(t)$, which is given by:

$$f(t) = \frac{\mathrm{d}\chi(t)}{\mathrm{d}t} \tag{4}$$

Then, Eq. 3 can be rewritten as:

$$P(t) = \varepsilon_0 \chi(0) E(t) + \varepsilon_0 \int_0^t E(\tau) f(t-\tau) \mathrm{d}\tau \tag{5}$$

The slow polarization is mathematically represented as the convolution between the input electric field and $f(t)$. This function characterizes how the material behaves upon subject to an electric field known as the dielectric response of the material. Applying an electric field $E(t)$ to a dielectric will generate a current density $j(t)$, which can be written as the sum of the conduction and polarization displacement current as [13]:

$$J(t) = \sigma_0 E(t) + \frac{\mathrm{d}}{\mathrm{d}t} D(t) \tag{6}$$

which gives

$$J(t) = \sigma_0 E(t) + \varepsilon_0(1+\chi(0))\frac{\mathrm{d}}{\mathrm{d}t}E(t) + \varepsilon_0\frac{\mathrm{d}}{\mathrm{d}t}\int_0^t f(t-\tau)E(\tau)\mathrm{d}\tau \tag{7}$$

The factor $(1+\chi(0))$ is the real part of the relative permitivity at high frequencies ε_∞.

If a sample of a purely linear dielectric material with a width d and area A is considered, the material can be modelled using a simple two parallel plates with a geometric capacitance C_0 that can be expressed as follows:

$$C_0 = \frac{\varepsilon_0 A}{d} \tag{8}$$

Assuming a uniformed electric field due to a step voltage with the amplitude of U_0, the electric field can be expressed as:

$$E(t) = \frac{U_0}{d} \tag{9}$$

Now, the current flowing from the high voltage plate to the other plate can be given as:

$$i(t) = \int_s J(t)\mathrm{d}A = J(t)\cdot A \tag{10}$$

Substituting Eq. 7 into Eq. 10 then using Eq. 8 and 9 yields:

$$i(t) = C_0\left[\frac{\sigma_0}{\varepsilon_0}U(t) + \varepsilon_\infty\frac{\mathrm{d}U(t)}{\mathrm{d}t} + \frac{\mathrm{d}}{\mathrm{d}t}\int_0^t f(t-\tau)E(\tau)\mathrm{d}\tau\right] \tag{11}$$

which can be rewritten in accordance to the applied voltage $U(t)$ as:

$$i(t) = C_0U_0\left[\frac{\sigma_0}{\varepsilon_0} + \varepsilon_\infty\delta(t) + \frac{\mathrm{d}}{\mathrm{d}t}\int_0^t f(t-\tau)E(\tau)\mathrm{d}\tau\right] \tag{12}$$

The delta function $\delta(t)$ is the derivative of the step function, which characterizes the rapid polarization/depolarization. Such current is known to feature larges and fast dynamics that are difficult to record in practice and often neglected. Thus, the polarization current can be expressed as [20]:

$$i_{\mathrm{pol}}(t) = C_0U_0\left[\frac{\sigma_0}{\varepsilon_0} + f(t)\right] \tag{13}$$

If the step voltage is removed and the testing dielectric is short-circuited at the time t_c, the insulation begins to depolarize, and the depolarization current i_{depol} can be measured. The sudden decrease of the applied voltage can be regarded as a negative step applied at the time t_c. The depolarization current can be expressed as [20]:

$$i_{\mathrm{depol}}(t) = -C_0U_0\left[f(t) - f(t+t_c)\right] \tag{14}$$

The principle of polarization and depolarization current can be further illustrated through Fig. 14 below:

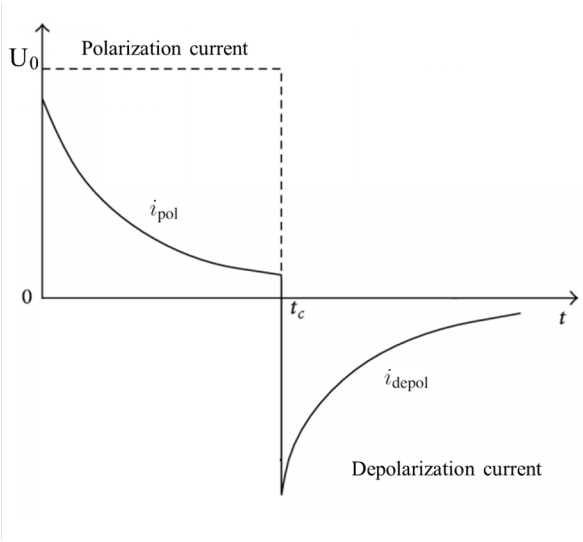

Fig. 14. Polarization/Depolarization current

Since $f(t)$ is a monotonically decaying function i.e. it decreases as t increases, then the second term of the depolarization current can be neglected if the charging time is long enough (t_c is large) and the depolarization current becomes proportional to the dielectric response function and the expression of the dielectric response becomes [20]:

$$f(t) = \frac{-i_{\text{depol}}(t)}{U_0 C_0} \tag{15}$$

B. Frequency Domain Polarization of dielectrics

The frequency-domain analysis for the current through the insulation in the frequency domain can be done by assuming an input voltage $U(\omega)$. Then, a Fourier transformation can be done to the current expression shown in (11) which yields:

$$I(\omega) = C_0 \left[\frac{\sigma_0}{\varepsilon_0} U(\omega) + j\omega\varepsilon_\infty U(\omega) + j\omega F(\omega) U(\omega) \right] \tag{16}$$

Fundamentally, the Fourier transform of the dielectric response is known to be the complex dielectric susceptibility $\tilde{\chi}$, which can be expressed as:

$$\tilde{\chi}(\omega) = \chi'(\omega) - j\chi''(\omega) = \int_0^\infty f(t) e^{-j\omega t} \mathrm{d}t \tag{17}$$

The total current in the dielectric material can be expressed as:

$$I(\omega) = j\omega C_0 \left[\varepsilon_\infty + \chi'(\omega) - j\left(\frac{\sigma_0}{\omega\varepsilon_0} + \chi''(\omega) \right) \right] U(\omega) \tag{18}$$

Which can be rewritten by replacing the complex dielectric susceptibility with complex permittivity as:

$$I(\omega) = j\omega C_0(\omega) \tilde{\varepsilon}(\omega) U(\omega) = j\omega \tilde{C}(\omega) U(\omega) \tag{19}$$

where

$$\tilde{\varepsilon}(\omega) = \varepsilon'(\omega) - j\varepsilon''(\omega) = \varepsilon_\infty + \chi'(\omega) - j\left(\frac{\sigma_0}{\omega\varepsilon_0} + \chi''(\omega) \right) \tag{20}$$

Separating $\varepsilon'(\omega)$ and $\varepsilon''(\omega)$

$$\varepsilon'(\omega) = \varepsilon_\infty + \chi'(\omega) \quad \text{Or} \quad \varepsilon'(\omega) = \varepsilon_\infty + \Delta\varepsilon'(\omega) \tag{21}$$

$$\varepsilon''(\omega) = \frac{\sigma_0}{\omega\varepsilon_0} + \chi''(\omega) \tag{22}$$

As for the complex capacitance, it can be defined as:

$$\tilde{C}(\omega) = C'(\omega) - jC''(\omega) = C_0\tilde{\varepsilon}(\omega) \tag{23}$$

Separating C' and C''

$$C'(\omega) = C_0\varepsilon'(\omega) \quad \text{Or} \quad C'(\omega) = C_\infty + \Delta C'(\omega) \tag{24}$$

$$C''(\omega) = C_0\varepsilon''(\omega) \tag{25}$$

The ratio of the loss current to the capacitive current is known as dielectric loss tangent $\tan\delta$, which is given as:

$$\tan\delta(\omega) = \frac{C''(\omega)}{C'(\omega)} = \frac{\varepsilon''(\omega)}{\varepsilon'(\omega)} \tag{26}$$

C. Dielectric response of Solid materials

Generally, the dielectric response of most solid insulating materials is linear. And, the dielectric response can be expressed using the following models [13]:

1) The Curie-von Schweidler (CvS) or fractional-power law is a universal model, which fits most solid insulation materials [21]. This response is expressed as:

$$f(t) = A_{\text{CvS}}t^{-n}, \qquad \text{where } 0 < n < 1 \tag{27}$$

2) The Debye function is used to reflect the response of a series RC circuit. The idea is to model the response obtained through several Debye functions:

$$f_{\text{Debye}}(t) = A_{\text{d}}e^{\frac{-t}{\tau}} \tag{28}$$

These models are used to fit a set of polarization/depolarization current measurements on solid insulation material. Multiple Debye or CvS terms can be stacked to obtain a better fit. Then, the complex permittivity is obtained by transformation of time domain response to the frequency domain using Fourier transformation $F(\omega)$. The transformation could be done analytically by solving the following integral [13]:

$$\mathfrak{F}\left[\mathrm{f(t)}\right] = \int_0^\infty f_{\text{Diel}}(t)e^{-j\omega t}\mathrm{d}t \tag{29}$$

Fortunately, the transformation of Curie-von Schweidler law and Debye function has been previously evaluated in many literatures such as [22] and [20] as follows:

$$F_{\text{CvS}}(\omega) = A_{\text{CvS}} \cdot \Gamma(1-n) \cdot \omega^{n-1}\left(\sin\left(\frac{n\pi}{2}\right) - j\cos\left(\frac{n\pi}{2}\right)\right) \tag{30}$$

$$F_{\text{Debye}}(\omega) = \frac{1}{C_0U_0}\sum_{i=1}^{k}\frac{A_{\text{d}_i}\tau_i - jA_{\text{d}_i}\omega\tau_i^2}{1+(\omega\tau_i)^2} \tag{31}$$

In (31) above, k is the number of the fitted Debye terms. The DC resistance R and geometric capacitance C_∞ can be measured by approximation. For complex geometries such as the stator coil, it is difficult to determine the geometric capacitance by analytical calculation.

Thus, it is recommended to experimentally estimate it by measuring the capacitance at the highest possible frequency. Then, from the PDC measurements, the DC resistance (R) can be approximated as [23]:

$$R = \frac{U_0}{i_{\text{pol}}(t_c)} \tag{32}$$

Finally, the curve fitting can be done either in the time domain using Eq. 27 and 28, or in frequency domain using Eq. 31 and 30. MATLAB has a curve fitting toolbox (cftools), which applies two of the most commonly used curve fitting algorithms, namely Levenberg-Marquardt and Trust-Region.

D. Numerical modelling of a real stator coil

In order to develop a model of the stator coil dielectric response, the effect of the overlapping region between the SCP and ECP is neglected. Then, the stator coil was split into two halves, and each part can be modeled using the distributed-element network shown in Fig. 15 below:

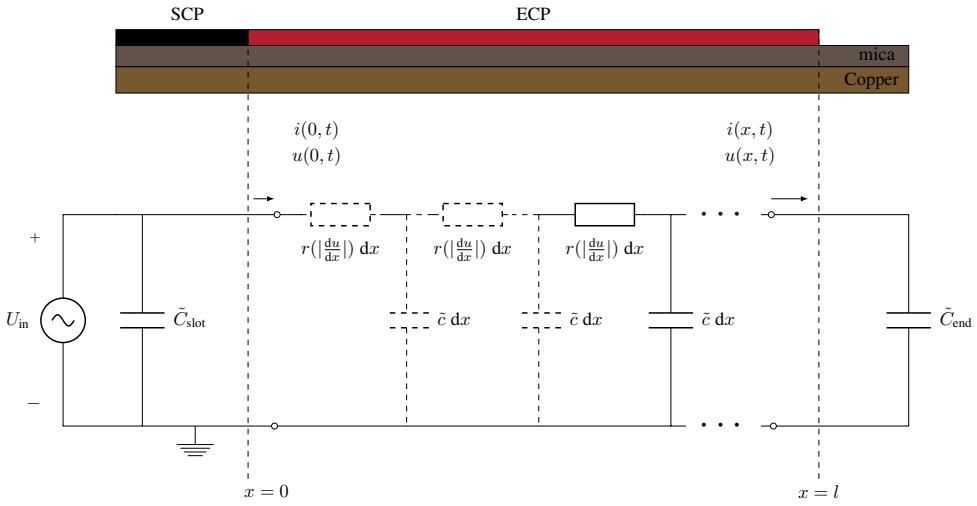

Fig. 15. Equivalent circuit of the coil end section

The coil portion shown above consists of a slot section and end section. The slot section can be modeled through the universal dielectric response for solid material (CvS) or Debye responses as discussed earlier. However, the unaged Epoxy mica insulation is known to have a good fit to the model given by [24]:

$$\tilde{C}_{\text{slot}} = C_\infty + A_{\text{CvS}}(j\omega)^{n-1} \tag{33}$$

In equation (33) above, the value of n and A_{CvS} are obtained from curve fitting the model above with a set of measurement data. As for the end section, the currents and voltages in the circuit shown in Fig. 15 will yield the following expressions:

$$\frac{\mathrm{d}u}{\mathrm{d}x} = -r\left(\left|\frac{\mathrm{d}u}{\mathrm{d}x}\right|\right) i(x,t) \tag{34}$$

The parameters r and c characterize the per unit length stress grading tape resistance and the per unit length capacitance under the stress grading layer. Additionally, the slow dielectric

response effect can be characterized in $\tilde{c}$, which yield the ECP layer surface current density to be expressed as:

$$\frac{\mathrm{d}i(x,t)}{\mathrm{d}x} = -C_0 \frac{\mathrm{d}}{\mathrm{d}t}\left[\varepsilon_\infty u(x,t) + \int_0^\infty f(\tau)u(x,t-\tau)d\tau\right] \tag{35}$$

If a *linear model* was considered, then the field dependency of r is neglected, and Fourier transformation would be applicable for the equations above which can be rewritten in the frequency domain as:

$$\frac{\mathrm{d}\tilde{U}}{\mathrm{d}x} = -r_0\tilde{I}(x,\omega) \tag{36}$$

$$\frac{\mathrm{d}\tilde{I}}{\mathrm{d}x} = -j\omega c\tilde{U}(x,\omega) \tag{37}$$

where r_0 is the per unit length stress grading tape resistance at 0 V/m. The analytical solution for the differential equations above matches the common expression used for modeling a long transmission line using distributed-element model. The characteristic impedance Z_0 and propagation constant γ are given by:

$$Z_0 = \sqrt{\frac{r_0}{j\omega c}} \tag{38}$$

$$\gamma = \sqrt{j\omega r_0 c} \tag{39}$$

Then, the complex capacitance can be computed from the input impedance as follow:

$$Z_{\text{in}} = Z_0 \frac{Z_{\text{end}} + Z_0 \tanh(\gamma l)}{Z_0 + Z_{\text{end}} \tanh(\gamma l)} \tag{40}$$

$$\tilde{C}(\omega) = \frac{1}{j\omega Z_{\text{in}}} \tag{41}$$

Obviously, it is expected that the result of this model may be a poor model, because the resistivity of ECP material is electric-field dependent. In other words, the surface conductivity would vary with position x, depending on the field distribution. If the linearity assumption is taken out by including field-dependent resistivity, then the *nonlinear model* can be developed. It is necessary to express the model in the time domain to consider the resulting harmonics. Thus, the nonlinear model can be expressed using the following PDE:

$$c\frac{\mathrm{d}U}{\mathrm{d}t} = \frac{\mathrm{d}}{\mathrm{d}x}\left[\frac{\mathrm{d}U}{\mathrm{d}x}\frac{1}{r_0}e^{\left(\eta\left|\frac{\mathrm{d}U}{\mathrm{d}x}\right|^p\right)}\right] \tag{42}$$

The equation above can be numerically solved using the MATLAB function pdepe, which considers a mix of Dirichlet and Neumann boundary conditions. If the applied potential is considered to be reversed, then the Dirichlet boundary condition would imply similar potential to the applied voltage U_{s} at the start of the grading part $x = 0$. This was done to simplify the expression. Then, the Neumann condition can set a zero current flow at the grading end where $x = l$. However, the initial guess can be either zero potential or the solution from the linear ODE.

The numerical solution obtained from this model is used to determine a vector of discrete samples of current into the grading at regular times. Preforming a discrete fourier transform on one or more whole cycles of this current will give the harmonics. From the resulting voltage and current vectors, the complex capacitance can be computed.

E. Summary

This chapter provided an explanation of the concepts behind the dielectric response, which is due to the polarization of dielectrics after being subjected to an electric field. The polarization feature can also be represented by frequency dependent relative permittivity and dielectric losses. In solid insulation materials, the dielectric response over a limited frequency range is often well approximated by the universal CvS function and appears as a straight line in the log-log scale [21]. However, this is not the case when stress grading materials are added to the insulation system. The addition of such material will introduce voltage dependent and nonlinear dielectric response. If a real stator coil is considered, then the straight section or the section that is covered with the slot corona protection layer can be modeled using CvS. Meanwhile, the end section can only be modeled by the PDE equation introduced previously.

CHAPTER V

DIELECTRIC RESPONSE MEASUREMENTS

Dielectric response measurements is the measure of the dielectric response of a particular medium over a range of frequencies. As discussed earlier, the dielectric response can be obtained either by the transformation of polarization/depolarization current data in the time domain or directly in the frequency domain. This chapter aims to illustrate the concepts of time and frequency domain measurements.

A. PDC Measurements

For PDC measurements, a DC voltage is applied to the one side of the insulation and the current meter is connected to the other side. Then, the polarization current is measured during the charging process, and then the depolarization current is measured after shorting the electrodes of test object. In order to perform tests at high voltages, a high voltage amplifier is considered. Since the measured current can be down to pA range, a very precise ammeter is required such as a feedback ammeter. The schematic used to measure the polarization and depolarization current is shown in Fig. 16:

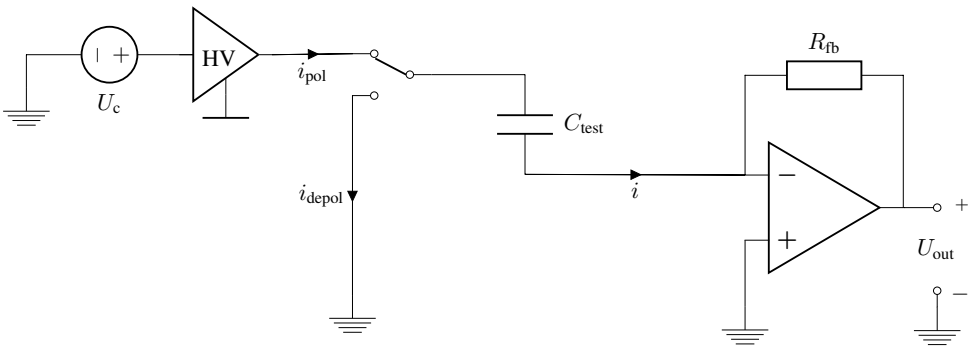

Fig. 16. Circuit schematic for PDC measurements

The measured current is given as:

$$i(t) = \frac{-U_{out}}{R_{fb}} \tag{43}$$

After acquiring the data of current over time, one can numerically transform the data to the frequency domain. It is more convenient to consider numerical approaches since it is easier to implement for various types of data. One numerical transformation example was presented and discussed in [25]. However, in order to achieve good transformation for frequencies below 1 Hz, the time domain data should be taken at least for 1000 s. Despite that, the method is still interesting for this thesis, since the influence of nonlinear stress grading material is more prominent in low frequency range.

B. Dielectric response measurement in frequency domain

The most common way to get the dielectric response in frequency domain is to generate a signal $U_{\text{in}}(\omega)$ and apply it one side of the insulation while taking the measurements from the other side. The measured the current $I(\omega)$ that flows through the insulation. Then, the complex capacitance can be calculated as:

$$\tilde{C}(\omega) = C'(\omega) - jC''(\omega) = \frac{I(\omega)}{j\omega U_{\text{in}}(\omega)} \tag{44}$$

An example of a basic FDS measurement circuit is shown in Fig. 17 below:

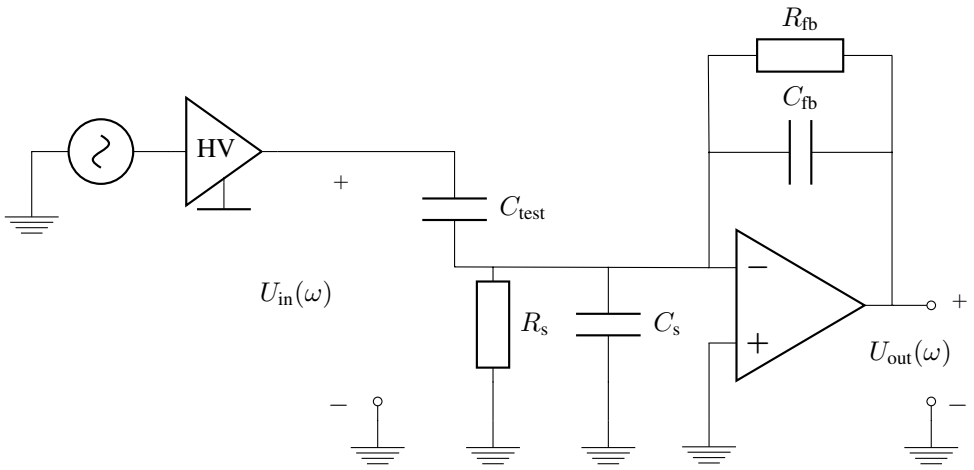

Fig. 17. An example of a basic FDS measurement circuit

For more practical presentation, two shunts elements are introduced, namely C_{s} and R_{s} to characterize the parasitic capacitance cable resistance of the test object, respectively. Assuming that the potential-shift is neglected, the measured complex capacitance can be expressed as:

$$\tilde{C}_{\text{test}}(\omega) = C'_{\text{test}}(\omega) - jC''_{\text{test}}(\omega) = \\ \frac{-U_{\text{out}}(\omega)}{j\omega U_{\text{in}}} \left[\left(\frac{1}{R_{\text{fb}}} + j\omega C_{\text{fb}} \right) + \frac{1}{H(\omega)} \left(\frac{R_{\text{fb}} + R_{\text{s}}}{R_{\text{fb}} R_{\text{s}}} + j\omega (C_{\text{s}} + C_{\text{fb}}) \right) \right] \tag{45}$$

The term $H(\omega)$ reflects the opamp gain. For an ideal amplifier, the gain is assumed to infinity leading to the impact of the shunts elements (R_{s} and C_{s}) to become negligible. As a result, Eq. 45 can be simplified to:

$$C'_{\text{test}}(\omega) + jC''_{\text{test}}(\omega) = \frac{-U_{\text{out}}(\omega)}{j\omega U_{\text{in}}(\omega)} \left[\left(\frac{1}{R_{\text{fb}}} + j\omega C_{\text{fb}} \right) \right] \tag{46}$$

C. Dielectric response measurement instruments

The measurements schematics shown previously in Fig. 16 and 17 were just examples of basic measurements schematics, which were presented for the purpose to measurement concepts illustrations. However, industrial FDS instruments has a far more complicated circuits that includes more features e.g., filters, protection elements and different earthing typologies. The instruments used in this thesis are described below:

- **Megger IDAX300 Insulation Diagnostic Analyzer**: One of state of the art measurement devices developed by Megger. The device can perform the PDC and DFR measurements over a wide range of frequencies for various types of high voltage equipment. The device is shown in Fig. 18 below:

Fig. 18. Megger IDAX300 insulation diagnostic analyzer [26]

A summary of some important of the technical parameters is shown below:

- Two power sources of 10 V and 200 V (peak values) with the maximum current output of 50 mA peak and frequency range DC - 10 kHz
- Capacitance measurements range $10\,\mathrm{pF}$ –$100\,\mu\mathrm{F}$.
- Inaccuracy of 0.1 mHz – 1 kHz sweep at 200 V:
  - $\geq$1000 pF: 0.5% of reading + 0.01% of full scale
  - $\geq$300 pF: 0.5% of reading + 0.02% of full scale
  - $\geq$10 pF: 0.5% of reading + 0.10% of full scale
- PDC Measurements have $\pm$ 50 mA peak output with 0.1 pA resolution and 0.5% $\pm$ 1 pA inaccuracy.

- **Megger VAX020 High voltage amplifier**: VAX 020 extends the IDAX test voltage range from 200 V to 2 kV. The device is shown in Fig. 19 below:

Fig. 19. Megger VAX020 high voltage amplifier [27]

A summary of some important of the technical parameters is shown below [27]:

– Voltage output range 0 - 2 kV (peak)

– Current rating of 40 mA (peak) above 50 Hz derating linearly to 30 mA below 10 Hz

– Capacitive load capability 0 – 20 µF, 80 nF at 2 kV and 50 Hz

– IDAX300 with VAX020 amplifier have inaccuracy for a 0.1 mHz – 1 kHz sweep at 2 kV (peak) of:

  * ≥1000 pF: 0.5% of reading + 0.01% of full scale
  * ≥300 pF: 0.5% of reading + 0.02% of full scale
  * ≥10 pF: 0.5% of reading + 0.03% of full scale

- **TREK 20C-HS voltage power amplifier**: TREK voltage amplifier is capable of taking the test voltage range up to 20 kV peak. The device is shown in Fig. 20 below:

Fig. 20. TREK 20 kV voltage amplifier [28]

A summary of some important of the technical parameters is shown below [27]:

- Output Voltage: 0 to ±20 kV DC or peak AC
- Output Current: 0 to ±20 mA DC or 60 mA peak AC for 1 ms
- Slew Rate: greater than $800\,\mathrm{V/\mu s}$
- Large Signal Bandwidth: DC to greater than 5.2 kHz (1% distortion)
- Gain: 2000 V/V Fixed

D. Practicalities in PDC measurements

PDC measurements can be performed by using simple devices, i.e. a high DC voltage source and an ammeter. Inherently, the insulation has high resistance, which leads to low leakage currents to be measured depending on the test object and its condition. PDC results are subject to error, especially as the current becomes small in long-time measurements. Thus, measurements of such currents can be affected by instrument noise and environment interference. Some potential noise sources that can affect the measurements are people's movements, noise of voltage source, ground disturbance caused by other equipment and test leads [29]. Another important factor to consider is the length and shape of the leads. However, the use of filters can help in reducing the noise. Such filters can be either analog or digital. If analog filters are considered, then capacitive filters should be kept minimal to avoid exhibiting the dielectric relaxation phenomena [29]. Digital filters can be a good alternative. The simplest algorithm that could be applied is the moving average. The moving average calculates the average data within a predefined window size k that slides within the set of data i, producing a new set of data i_{filtered}, which can be expressed according to the following equations:

$$i_{\text{filtered}}(t) = \frac{1}{k}\left[i(t) + i(t-1) + ... + i(t-(k-1))\right] \tag{47}$$

An example of PDC measurements before and after applying the filter is shown in Fig. 21 below:

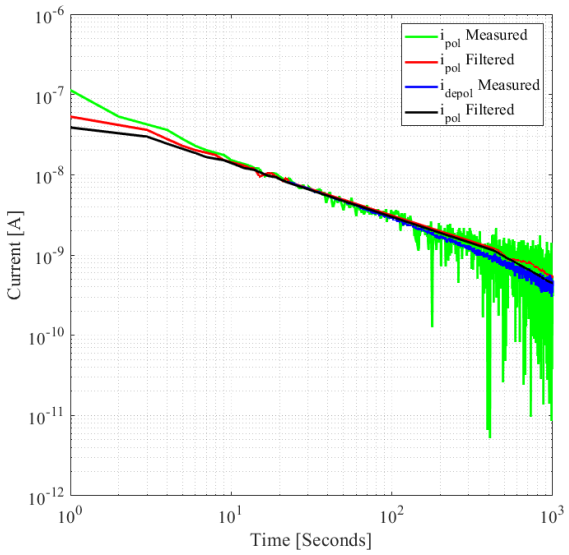

Fig. 21. PDC measurements before and after applying digital filter

E. Practicalities in FDS measurements

The IDAX and VAX are designed to be fully compatible and the output voltage from VAX amplifier is measured. However, the TREK amplifier available for this work was not configured with a voltage divider that would permit the IDAX to get a measurement of the voltage at the TREK output. Some phase and correction between the IDAX output and the TREK output is therefore needed, besides amplitude scaling. The phase correction based

on using a standard capacitor (air dielectric) as a reference to measure the phase deviation of $\Delta\delta$, as shown in Fig. 22 below:

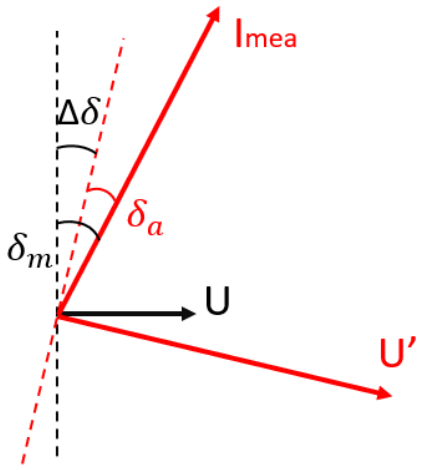

Fig. 22. Concept of phase shift correction

Based on this concept, one can measure the capacitance and the corrected dielectric response respectively according to the following expressions:

$$C_{\mathrm{a}} = \frac{C_{\mathrm{m}}}{H} \tag{48}$$

$$\tan(\delta_{\mathrm{a}}) = \tan(\delta_{\mathrm{m}} - \Delta\delta) \tag{49}$$

Where

- C_{a} and δ_{a} are the actual corrected values
- C_{m} and δ_{m} are the measured values
- H is the amplifier gain
- $\Delta\delta$ is the phase deviation from the amplifier

F. Summary

In this chapter, the concept of dielectric response measurement, both in the time domain and frequency domain was described. The time-domain measurement consists of measuring the polarization/depolarization current on the surface of the measuring electrode, then using Fourier transformation to obtain the dielectric response. However, the accuracy of this approach is limited by the linearity of the insulation system, i.e. it is not valid for insulation systems with nonlinear materials such as SiC tape. It is therefore more convenient, for the purpose of this thesis, to consider the direct FDS results to be the main reference when identifying the influence of ECP or assessing the numerical models introduced in chapter IV.

CHAPTER VI

TESTING FOR PRACTICAL STATOR COILS

Two 6.6 kV commercial stator coils were tested based on applying the concepts stated in the previous chapters. The test results of dielectric response measurement are included in this chapter.

A. *Test Object*

The commercial stator coils were supplied by ABB, with a nominal operating voltage of 6.6 kV. One of them had a 125 mm long ECP layer made of SiC tape while the other doesn't have the ECP layer. The main insulation of the coils consists of 6 half-lapped layers of mica tape. Dimensions of the stator coils are shown in Fig. 23 below:

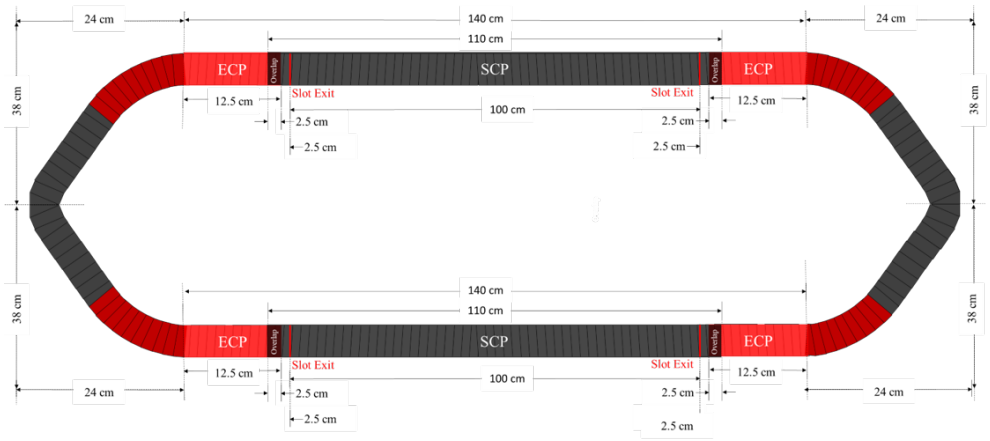

Fig. 23. Dimensions of the stator coil sample

The other coil without ECP tape has similar dimensions to the coil shown in Fig. 23 except for a slight difference in thickness (around 1 mm) due to the absence of ECP tape.

The cross sections of the stator coil is shown in Fig. 24 below:

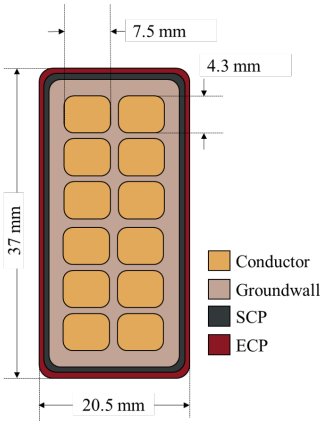

Fig. 24. Cross sections of the stator coils

B. Dielectric response measurement experiment setup

A measuring electrode was formed by wrapping the straight section of the coil with copper tape. The copper shield is about 1.37 m long. Then, three different experiments were designed to measure the dielectric response of the stator coil samples. The IDAX300 and VAX020 were used to measure the dielectric response at various voltages up to 2 kV. For higher voltages, the IDAX300 was used as an input source of the TREK 20C-HS, which extends the voltage range up to 20 kV.

The connection diagram for dielectric response measurement below 2 kV is shown in Fig. 25 below:

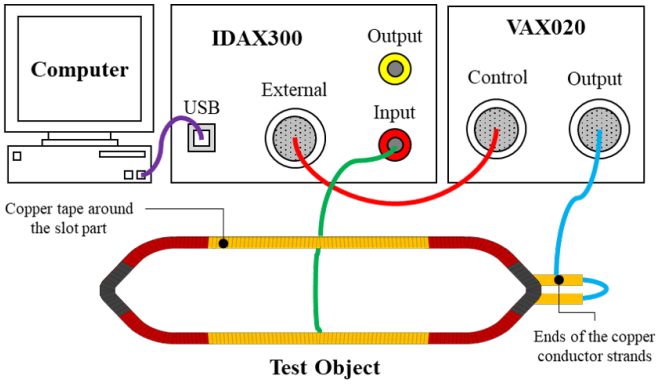

Fig. 25. Connection diagram of dielectric response measurement under 2 kV

Since both IDAX300 and VAX020 are manufactured by Megger, they are compatible with each other and the test voltage can be easily controlled by software. This combination can also be used to perform the PDC measurement.

The connection diagram for dielectric response measurement below 20 kV is shown in Fig. 26 below:

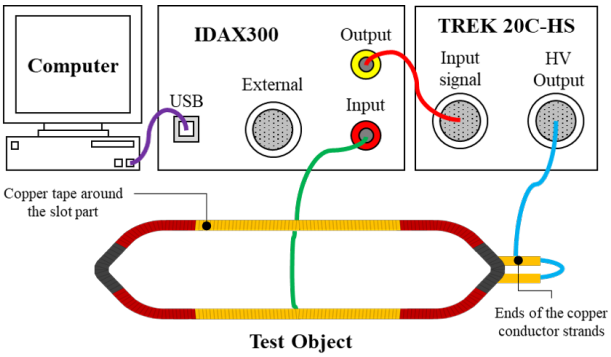

Fig. 26. Connection diagram of dielectric response measurement under 20 kV

The TREK output is controlled using the IDAX300 output with the amplifying factor of 2000, i.e. if the desired voltage is 4 kV then the voltage output from the IDAX is set to 2 V. The laboratory setup for measuring the dielectric response of the stator coils can be seen in Fig. 27 below:

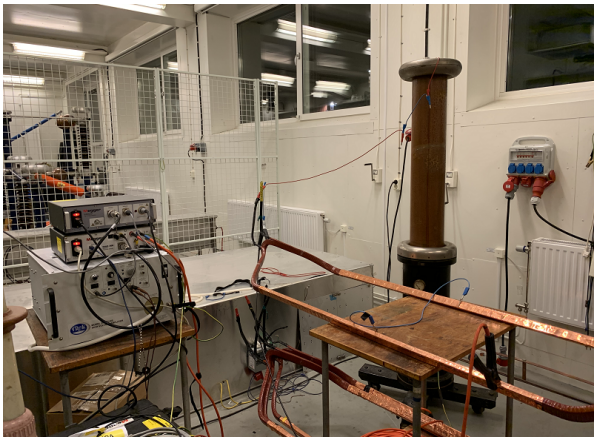

Fig. 27. Setup of the first two experiment to measure the dielectric response

For the time domain measurement, the polarization current was measured at 140 V and 1400 V for a duration of 10000 s. Following that, the strands were grounded and the depolarization current was measured for a period of 10000 s. For the frequency domain measurements, AC voltages with peak values of 20 V, 200 V, 2 kV, 4 kV, 6 kV, 8 kV and 10 kV were applied to the both coils having frequencies ranging from 0.1 mHz to 100 Hz. The IDAX300 provides several test modes for dielectric response testing, e.g. Grounded Specimen Test (GST) and Ungrounded Specimen Test (UST). The UST mode was used for this study.

C. Time domain results

The PDC measurements were taken over 10000 s with resistive and capacitive feedback of 1 GΩ and 1 pF respectively. The results obtained are shown in Fig. 28 below:

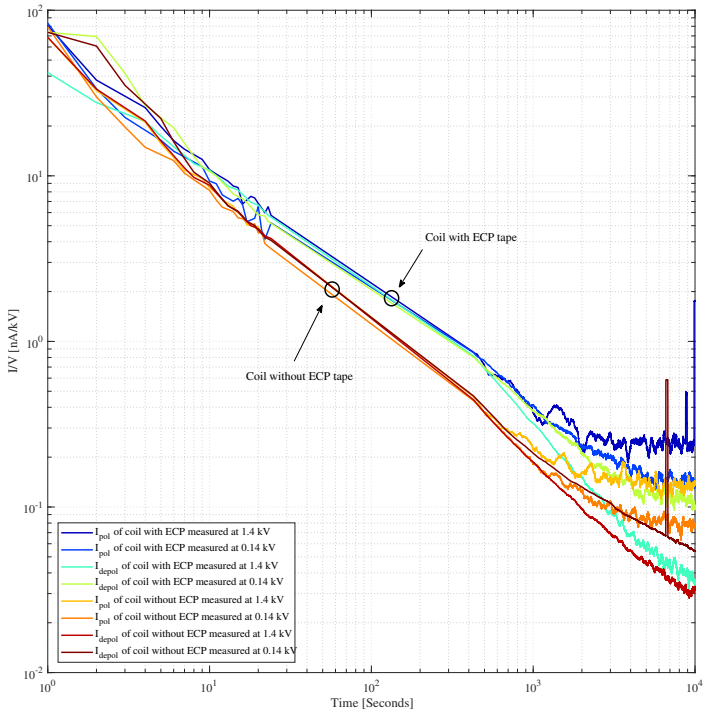

Fig. 28. PDC measurements of the tested coils

From Fig. 28 above, it can be concluded that the measured polarization and depolarization current is higher for the coil with ECP tape. Also, the polarization and depolarization current are observed to be different at different test voltage despite the ordinate being scaled by the applied voltage.

The polarization current has shown to reach higher magnitude as the test voltage goes higher. In the other hand, the opposite occurs for the depolarization current. It can be also seen that depolarization current decays ¨faster¨ when the charging voltage is higher.

The fast Fourier transformation was done on the PDC measurements using the same algorithm discussed in [25]. Then, the complex capacitance was calculated and compared to the FDS measurements as shown in Fig. 29 below:

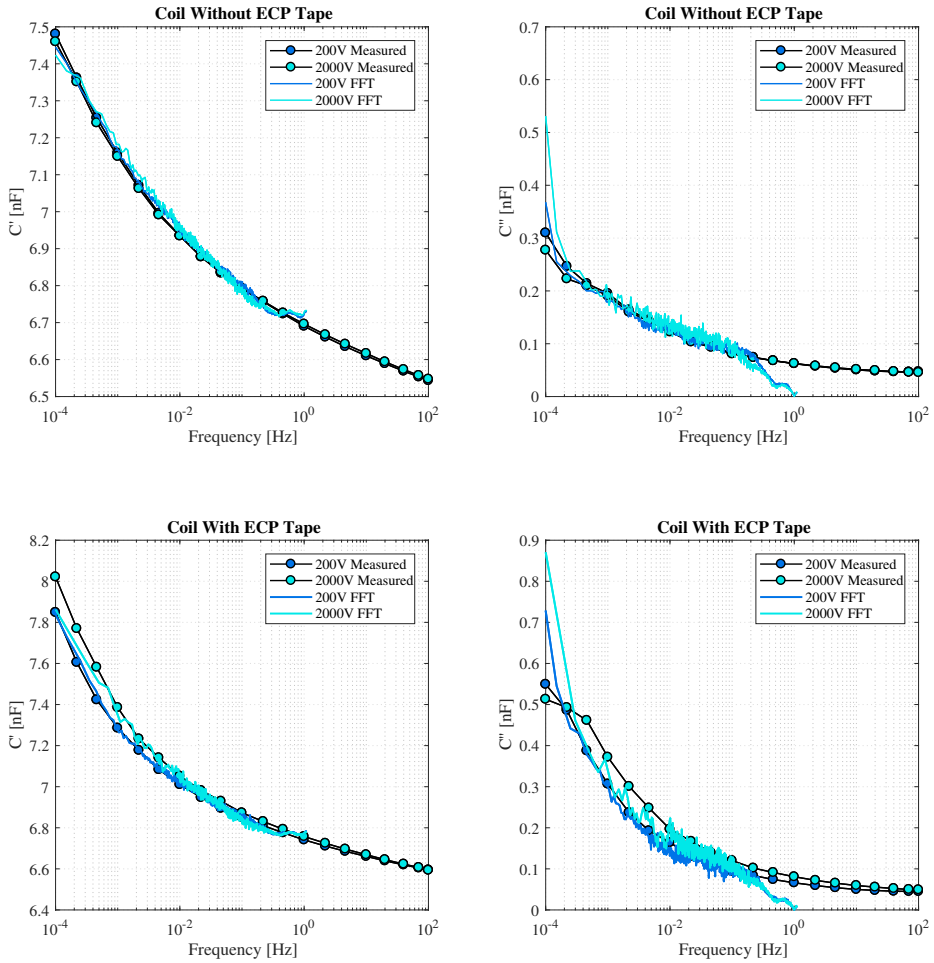

Fig. 29. A comparison of complex capacitance obtained from FFT of i_{pol} against direct frequency-domain measurement

From Fig. 29 above, it can be seen that the transformation works well within the frequency range $10^{-4} - 10^{-1}$ Hz. Additionally, the Fourier transformation gives better matching results to the coil without the ECP layer than the one which has it. This is expected since fundamentally, the Fourier transformation is supposed to be used for linear systems, which is not the case for the coil with ECP. Thus, the transformation can not reflect the voltage impact on the nonlinear system.

D. Frequency domain results

The wrapped copper shield acting as the measurement electrode covers the straight bar section, including the slot part and the slot exit area covered with ECP tape. Then, DFR measurements were performed at various voltages over the frequency range from 10^{-4} Hz up to 10^{2} Hz. The results are shown in Fig. 30 below:

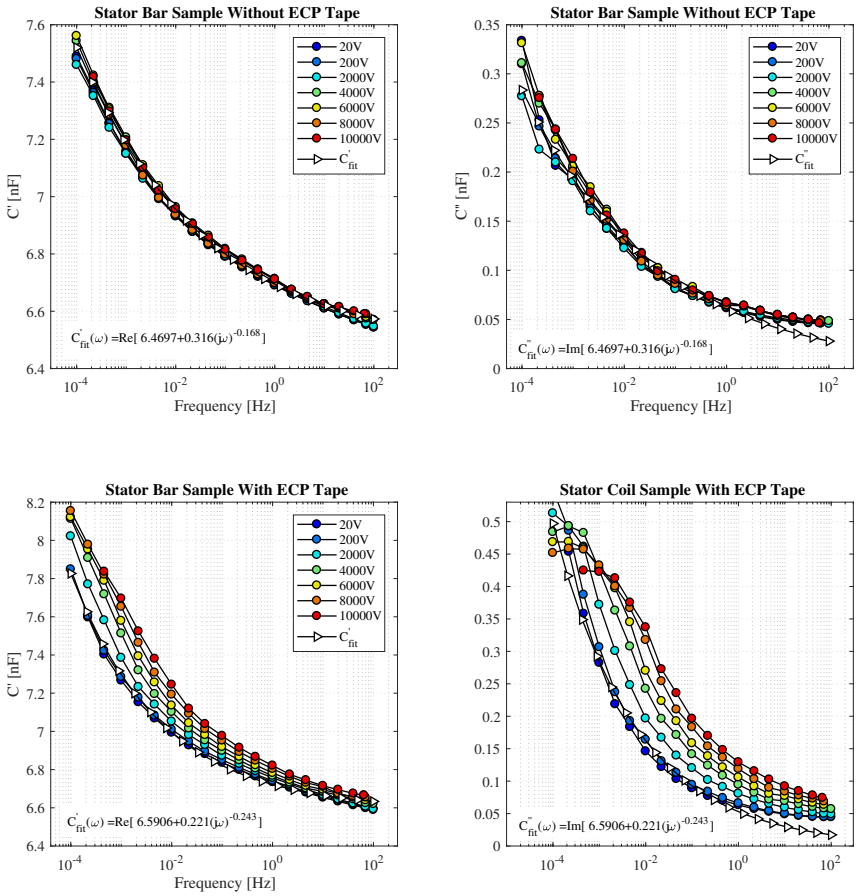

Fig. 30. FDS measurements of the tested coils

It can be seen from Fig. 30 above, that the dielectric response of the coil without ECP has a slight voltage dependent characteristic compared to the coil with ECP. The difference is due to the coil's insulation system without ECP, mostly consisting of mica, which has a dielectric response with negligible voltage dependence. Also, it should be noted that another source of variation between both coils measurements is the slight geometry change between the two tested coils due to losing around 1 mm of ECP thickness.

Moreover, the results have shown to have an excellent fit to the model of $C_{\infty} + b(j\omega)^{n-1}$ nature beside a slight deviation when frequencies above 1 Hz and extremely low frequencies at higher test voltages. This might be due to measurement error caused by the noise from the high voltage amplifier. The parameters used to fit the measured data are shown in Table II below:

TABLE II
FDR MEASUREMENTS FITTING PARAMETERS

Parameter	Coil with ECP	Coil without ECP
C_∞[nF]	6.5906	6.4697
b[nF]	0.22143	0.31586
n	0.75658	0.83222

As for the coil sample with ECP tape, the voltage dependent dielectric response can be clearly seen as the test voltage goes higher and the change of frequency of the loss peak. Because of this voltage dependent property, the linear model proposed in previous sections can no longer be considered suitable to model a bar sample with ECP.

E. Influence of ECP tape

The dielectric response due to ECP's presence can be calculated by subtracting the dielectric response of the coil without ECP from the coil with ECP. The calculated dielectric responses at various voltages are shown in Fig. 31 below:

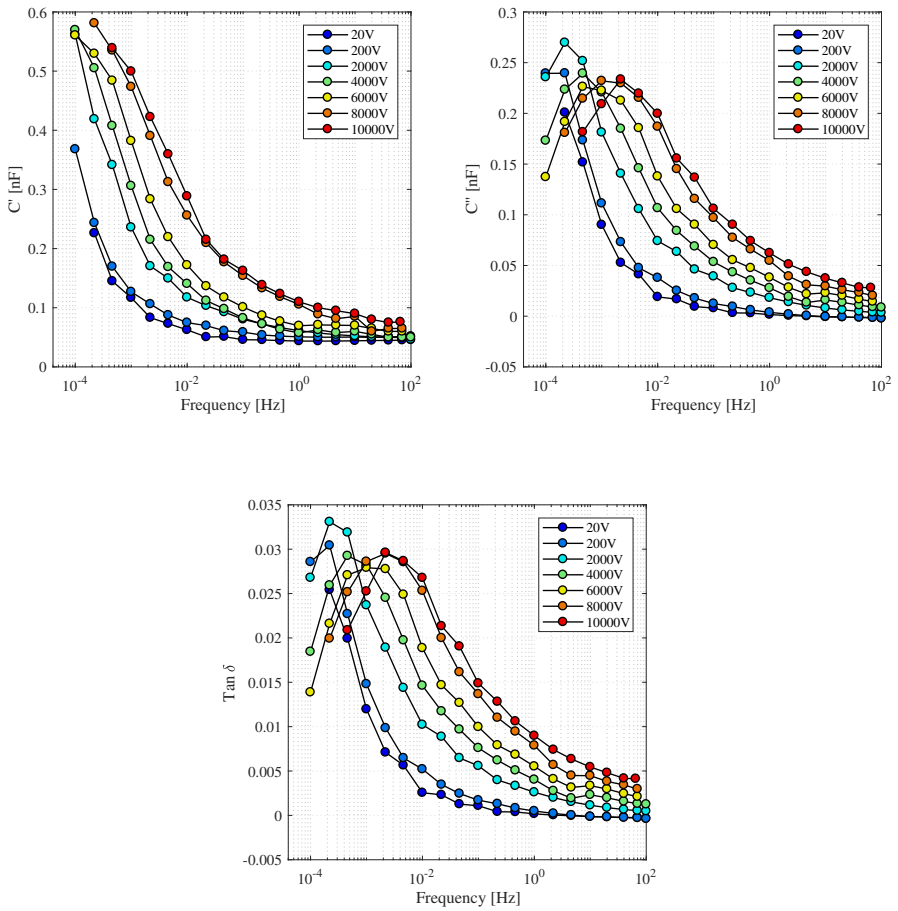

Fig. 31. Calculated dielectric responses due to the ECP's presence at various voltages

According to Fig. 31, it can be observed that the increase of voltage will cause the loss peak to shift towards higher frequencies. Additionally, there is only slight difference between measurements at 8 kV and 10 kV, which might indicate that the ECP tape conductivity reaches a saturation region, i.e. the conductivity tends to become constant when the electric field reaches a certain threshold. The slight difference between the measurements at 20 V and 200 V is because the electric field is very low for both voltage levels.

The linear and nonlinear numerical models of the coil end section discussed previously in section D of chapter IV were used to compare with actual measurements, results are shown in Fig. 32 below:

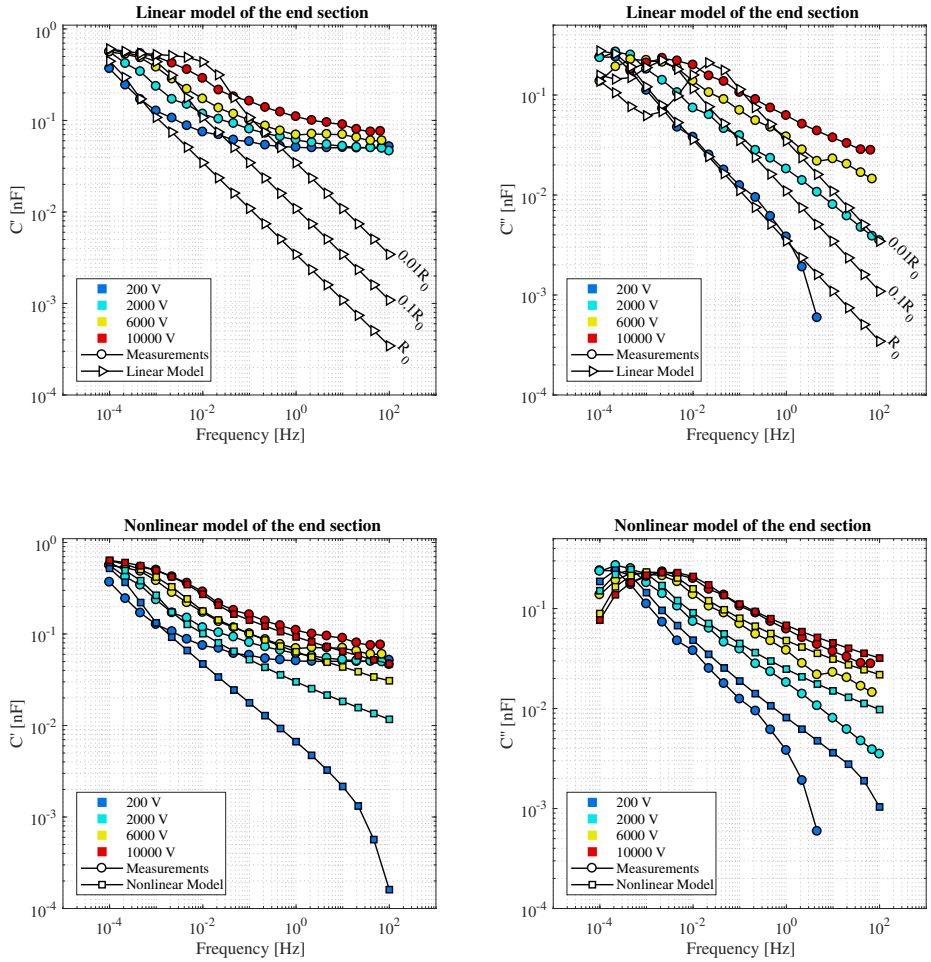

Fig. 32. Results obtained from numerical models of end section at various voltages

From Fig. 32 above, it can be seen that the nonlinear model has a better fit to the measured results. On the other hand, the nonlinear model tends to deviate from the measurement results as the frequency increases, especially at lower voltages. However, the linear distributed model has shown to have good fit on a few points near the loss peak frequency.

The parameters used for linear and nonlinear distributed models are summarized in Table III below:

TABLE III
PARAMETERS FOR LINEAR AND NONLINEAR DISTRIBUTED-ELEMENT MODELS

Linear distributed-element Model		
Parameter	**Value**	**Description**
l_{c}	2.8 [m]	Length of the measurement electrode
C_∞	6.5433 [nF]	These parameter were set based on curve fitting the stator coil without ECP tape
b	0.31584 [nF]	
n	0.83222	
$c_m(\omega)$	$\frac{1}{l_{\mathrm{c}}} C_\infty + b(j\omega)^{n-1}$ [nF]	
Nonlinear distributed-element Model		
l_{SG}	0.1 [m]	Length of Stress Grading region
σ_0	1.15×10^{-14} [S]	Geometric surface conductivity of ECP tape according to [30]
r_{p}	5.3 [GΩ/m]	Per unit length surface resistance estimated from PDC measurements using Eq. 32
E_0	16070 [V/m]	ECP tape model coefficient according to [30]
p	0.66	ECP tape model coefficient according to [30]
C_{end}	$0.01 l_{\mathrm{c}} c_{\mathrm{m}}(\omega)$ [nF]	Assumed to be the 1% of the straight portion [24]
$c_{\mathrm{p}}(\omega)$	$c_{\mathrm{m}}(\omega) + c_{\mathrm{e}}(\omega)$ [nF]	$c_{\mathrm{e}}(\omega)$ is the per unit length capacitance of the ECP response over the length of 10 cm

F. Summary

The dielectric response of an insulation system can be measured in the time domain or frequency domain. The ECP layer within the stator coil insulation system introduces nonlinearity to the dielectric response. This nonlinearity can be characterized by the dielectric response as a function of the testing voltage.

The complex capacitance due to ECP tape's presence was calculated by subtracting the coil's capacitance without ECP from the coil with ECP. Moreover, a linear and nonlinear distributed-element model were considered to model the nonlinear behavior due to the ECP. The nonlinear model was observed to provide a better fit than the linear model.

CHAPTER VII

FEM SIMULATION OF THE STATOR COIL

FEM simulation is commonly used in engineering to solve complex problems that involve analyzing multiple physics principles and complex geometry, which are typically difficult to evaluate analytically. This chapter is dedicated to discussing the FEM simulation of the stator coil end section.

A. Background and Objective

The numerical models introduced in section D of chapter IV only accommodated the one dimension of the stator coil i.e. variations in potential were only considered along the axial length of the ECP (10 cm). Introducing more actual parameters such as the thickness of the ECP and other insulation layers will result in a more complex model. The finite element method (FEM) is a powerful tool to do the analysis for systems with multi-dimensional geometry. The general concept of FEM solver is to solve the partial differential equations while considering three space variables through ”discretisation”, i.e. breaking down the complex geometry into smaller parts or elements. Elements size can be controlled by controlling the Mesh type and size. One software for finite element analysis is COMSOL Multiphysics. It allows the user to create or import 2D or even 3D geometries easily and then choose the type of physics related to the problem. Additionally, COMSOL provides a number of studies e.g. time domain, frequency domain and small-signal analysis. For this thesis, the objective is to use COMSOL to implement a more detailed model than the ones introduced in section D of chapter IV and to use this to study the electric field and voltage distribution on the ECP layer surface.

B. Setting up the FEM model for the slot exit area

In this study, the coil end section was modelled as a cylinder using 2D Asymmetric geometry: this approach consists in setting the radius of different insulation layers to match the area of the same particular layer in 2D cross section. The geomerty used in this approach can be seen in Fig. 33 below:

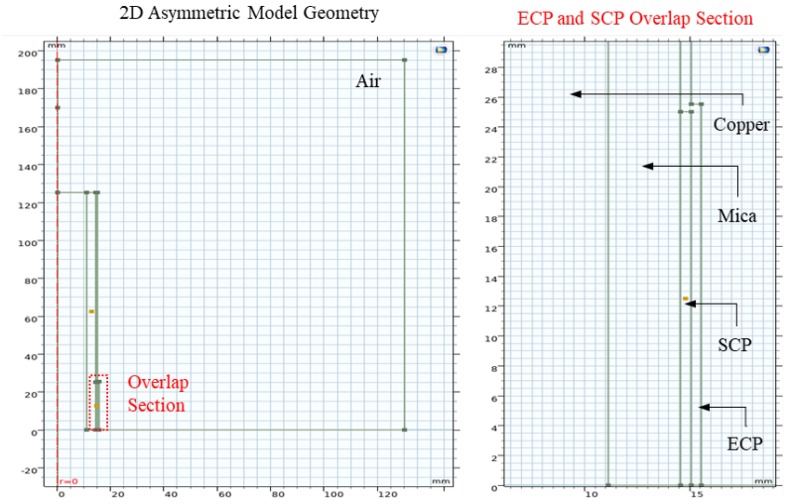

Fig. 33. 2D asymmetric model for the slot exit area

Each line connecting two points forms a boundary. A region enclosed by several boundaries creates the ”Domain”. Each domain must be assigned with a material which has relevant properties according to the selected physical model. If electric current (ec) physics is added, then materials properties are characterized by electrical conductivity σ and relative permittivity ε_{r}. The materials and their properties used in this simulation are described in Table IV below:

TABLE IV
MATERIALS PROPERTIES USED IN FEM SIMULATION

Material	Electrical Conductivity σ [S/m]	Relative permittivity ε_{r}
Copper	5.998×10^{7}	1
mica	2×10^{-15}	6
Carbon	10^{-2}	15
SiC	$\left[1.15 \cdot 10^{-14}\right] \exp\left[\frac{\lvert E\rvert}{16070}\right]^{0.66}$	10

The boundaries assigned to the models are shown in Fig. 34 below:

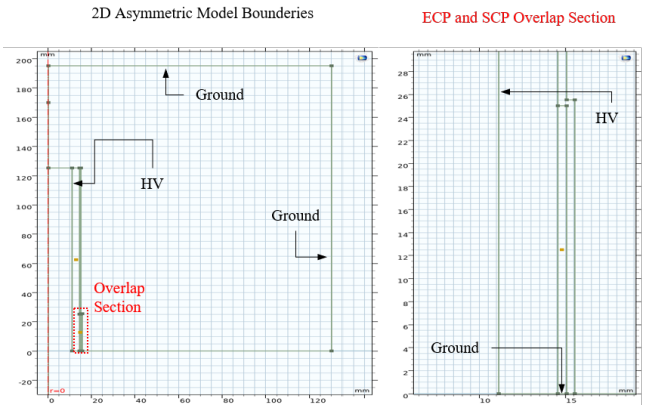

Fig. 34. FEM models boundaries

C. Surface Electric Field and Voltage distribution

A hyphenate frequency-domain domain study was considered to investigate the surface electric field and voltage distribution on the ECP layer. One of the limitations of this type of study arises from that it works with sinusoidal values rather than the interaction of instantaneous electric-field and current values as done in the time domain study. However, the frequency-domain study can be used as an approximation to take advantage of the rapid calculation feature. The results obtained from the 2D asymmetric model are shown in Fig. 35 below:

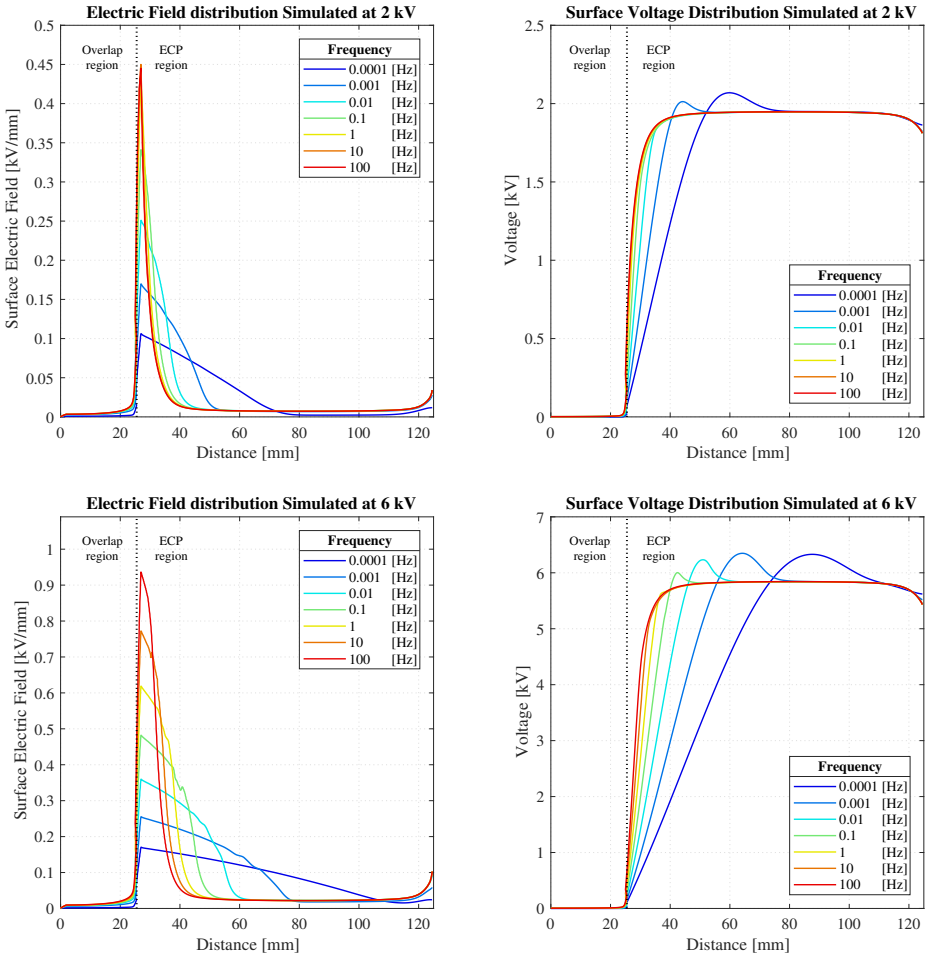

Fig. 35. ECP surface electric field and voltage distribution using 2D asymmetric model

From Fig. 35, it can be concluded that peak electric stress occurs within the overlapping region. As the frequency decreases, the surface peak value reduces, and the electric stress concentration is distributed along the ECP region.

CHAPTER VIII

CONCLUSION

This thesis work has shown that applying the ECP design significantly reduces the PD activity and increases the inception voltage. However, the use of the ECP introduces nonlinearity in the dielectric response, i.e. voltage dependent dielectric response in the stator coil insulation system. The linear response is determined by the property of the main insulating material, which is non-impregnated mica tape. On the other hand, the nonlinear part is dependent on the properties of SiC material as well as the underlying mica tape and their geometry.

The dielectric responses of one stator coil with ECP tape and another one without ECP tape were measured in both the time and frequency domain. Performing FFT on PDC measurements has shown that the transformation from time to frequency domain works well at frequencies lower than 1 Hz for linear dielectrics, e.g. the coil sample without ECP. However, the transformation of the coil sample with ECP tape measurements was not able to accommodate the voltage dependency factor and thus it is subject to error.

In order to show a frequency-domain view of the nonlinear system, it is better to measure directly in the frequency-domain using DFR measurements. Under the assumption that two coils samples have the same designed parameters except that one has an extra ECP layer, the dielectric response of SiC tape was obtained by subtracting the DFR results of the coil without ECP from the sample with ECP. The voltage dependent dielectric response of SiC was observed. As the voltage goes higher, the loss peak tends to shift towards higher frequencies.

Regarding the coil insulation system modeling, the nonlinear distributed-element model has shown to have an excellent fit to the measured data at low frequencies. Meanwhile, the linear distributed-element model has shown to provide a good fit at a few points around the loss peak frequency if the resistance multiplier is adjusted to imitate the voltage dependency, as the linear model alone cannot accommodate the field-dependent resistivity of SiC.

The FEM simulation done in this thesis was limited to the electric field analysis of a simple 2D asymmetric geometry. However, a more detailed 3D model is recommended for the scope of future work. Additionally, it would be interesting to see a comparison between the evaluated complex capacitance from FEM simulation and the measured results.

REFERENCES

[1] G. C. Stone, I. Culbert, E. A. Boulter, and H. Dhirani, *Electrical insulation for rotating machines: design, evaluation, aging, testing, and repair*. John Wiley & Sons Inc., 2014.

[2] CIGRE, *Hydrogenerator Failures – Results of the Survey*. Paris, France: CIGRE, 2003.

[3] N. Taylor, *Dielectric response and partial discharge measurements on stator insulation at varied low frequency*. PhD thesis, KTH, Electromagnetic Engineering, 2010.

[4] M. Znidarich, "Hydro generator high voltage stator windings: Part 2 - design for reduced copper losses and elimination of harmonics," *Australian Journal of Electrical and Electronics Engineering*, vol. 5, no. 2, pp. 119–135, 2009.

[5] E. Boulter and G. Stone, "Historical development of rotor and stator winding insulation materials and systems," *IEEE Electrical Insulation Magazine*, vol. 20, pp. 25 – 39, 06 2004.

[6] W. Deer, R. Howie, and J. Zussman, *An Introduction to the Rock Forming Minerals*. London, United Kingdom: Mineralogical Society of Great Britain & Ireland, 2013.

[7] R. Chauhan, M. Singh, and B. Singh, "Rotating machine insulation materials and techniques - an overview," *Indian Journal of Engineering and Materials Sciences*, vol. 7, pp. 370–374, 10 2000.

[8] N. Andraschek, A. J. Wanner, C. Ebner, and G. Riess, "Mica/epoxy-composites in the electrical industry: Applications, composites for insulation, and investigations on failure mechanisms for prospective optimizations," *Polymers*, vol. 8, pp. 201–224, 05 2016.

[9] R. Vogelsang, T. Weiers, K. Fröhlich, and R. Brütsch, "Electrical breakdown in high voltage winding insulations of different manufacturing qualities," *IEEE Electrical Insulation Magazine*, vol. 22, pp. 5–12, 06 2006.

[10] YMMIE, "Vacuum Pressure Impregnation (VPI) plant." , November 15, 2019. Accessed on: July 12, 2020. [Online]. Available: https://web.archive.org/web/20191115080240/www.ymmie.com/html_products/Vacuum-Pressure-Impregnation-(VPI)-plant-562.html.

[11] Sloanelectric, "What Is Vacuum Pressure Impregnation?." , January 5, 2020. Accessed on: July 12, 2020. [Online]. Available: https://web.archive.org/web/20191103060911/www.sloanelectric.com/vacuum-pressure-impregnation-services/.

[12] IEC, "High-voltage test techniques – partial discharge measurements," *IEC std. 60270:2015*, 2015.

[13] E. Kuffel, W. S. Zaengl, and J. Kuffel, *High voltage engineering fundamentals*. Butterworth-Heinemann, 2000.

[14] R. Brütsch and T. Hillmer, "Corona protection in rotating high voltage machines," in *Proceedings of INDUCTICA 2006 Conference*, (Berlin, Germany), 2006.

[15] Quartzelec, "Stress Grading." , Oct 7, 2019. Accessed on: July 7, 2020. [Online]. Available: https://www.youtube.com/watch?v=ukrAdTVKhu8.

[16] IEC, "Rotating electrical machines - part 27-1: Off-line partial discharge measurements on the winding insulation," *IEC std. 60034-27-1:2017*, 2017.

[17] C. Hudon and M. Belec, "Partial discharge signal interpretation for generator diagnostics," *IEEE Transactions on Dielectrics and Electrical Insulation*, vol. 12, pp. 297–319, April 2005.

[18] Y. Luo, Z. Li, and H. Wang, "A review of online partial discharge measurement of large generators," *Energies*, vol. 10, no. 11, 2017.

[19] C. C. Tin, V. Madangarli, E. Luckowski, J. Casady, T. Isaacs-Smith, J. R. Williams, R. W. Johnson, G. Gradinaru, and T. S. Sudarshan, "Electric field breakdown mechanisms in high power epitaxial 4h-sic p-n junction diodes," in *ICSE '96. 1996 IEEE International Conference on Semiconductor Electronics. Proceedings*, pp. 55–58, Nov 1996.

[20] J. Liu, D. Zhang, X. Wei, and H. Karimi, "Transformation algorithm of dielectric response in time-frequency domain," *Mathematical Problems in Engineering*, pp. 1–7, 2014.

[21] A. Jonscher, "The universal dielectric response and its physical significance," *IEEE Transactions on Electrical Insulation*, vol. 27, no. 3, pp. 407–423, 1992.

[22] A. Shayegani, E. Gockenbach, H. Borsi, and H. Mohseni, "Investigation on the transformation of time domain spectroscopy data to frequency domain data for impregnated pressboard to reduce measurement time," *Electrical Engineering*, vol. 89, no. 1, pp. 11–20, 2006.

[23] A. Kuchler, *High Voltage Engineering: Fundamentals - Technology - Applications*. Heidelberg: Springer, 2018.

[24] E. David and L. Lamarre, "Low-frequency dielectric response of epoxy-mica insulated generator bars during multi-stress aging," *IEEE Transactions on Dielectrics and Electrical Insulation*, vol. 14, no. 1, pp. 212–226, 2007.

[25] J. Cheng, P. Werelius, and N. Taylor, "Temperature influence on dielectric response of rotating machine insulation and its correction," in *NORD-IS 19 Proceedings of the 26th Nordic Insulation Symposium*, pp. 145–149, Aug 2019.

[26] Megger, "IDAX300/350 - INSULATION DIAGNOSTIC ANALYZER." Accessed on: July 12, 2020. [Online]. Available: https://us.megger.com/insulation-diagnostic-analyzer-idax-series.

[27] Megger, "VAX020 - HIGH VOLTAGE AMPLIFIER." Accessed on: July 12, 2020. [Online]. Available: https://us.megger.com/high-voltage-amplifier-vax020.

[28] TREK, "Trek model 20/20C-HS." , November 20, 2019. Accessed on: July 12, 2020. [Online]. Available: https://web.archive.org/web/20191120164951/www.trekinc.com/products/20-20Chs.asp.

[29] T. Saha and P. Purkait, "Investigating some important parameters of the PDC measurement technique for the insulation condition assessment of power transformer," in *Proceedings of The Sixth International Power Engineering Conference (IPEC2003)*, pp. 367–377, 2003.

[30] N. Taylor, "Measured and modeled capacitance, loss and harmonics in stator insulation with nonlinear stress control," *IEEE Transactions on Dielectrics and Electrical Insulation*, vol. 22, no. 6, pp. 3133–3145, 2015.

CHAPTER IX

Appendix

A. Linear distributed-element model Matlab Code

```
%%%%%%%%%%%%%%%%%%%%%%%%%%%%%%%%%%%%%%%%%%%%%%%%%%%%%%%%%%%%%%%%%%%%%%%%%%%%
% Slot End Section Linear Model
%%%%%%%%%%%%%%%%%%%%%%%%%%%%%%%%%%%%%%%%%%%%%%%%%%%%%%%%%%%%%%%%%%%%%%%%%%%%
% By Amar Abideen - June 2020
%%%%%%%%%%%%%%%%%%%%%%%%%%%%%%%%%%%%%%%%%%%%%%%%%%%%%%%%%%%%%%%%%%%%%%%%%%%%
% Credit: This code was rewritten based on Nathaniel Taylor
% previous code during his PhD work
%%%%%%%%%%%%%%%%%%%%%%%%%%%%%%%%%%%%%%%%%%%%%%%%%%%%%%%%%%%%%%%%%%%%%%%%%%%%
% This Code was written to implement the nummerical model
% of a stator coil sample
%%%%%%%%%%%%%%%%%%%%%%%%%%%%%%%%%%%%%%%%%%%%%%%%%%%%%%%%%%%%%%%%%%%%%%%%%%%%
%%%%%%%%%%%%%%%%%%%%%%%%%%%%%%%%%%%%%%%%%%%%%%%%%%%%%%%%%%%%%%%%%%%%%%%%%%%%
% Note:
%%%%%%%%%%%%%%%%%%%%%%%%%%%%%%%%%%%%%%%%%%%%%%%%%%%%%%%%%%%%%%%%%%%%%%%%%%%%
% The assumptions made:
%1- ECP resistivity is independent of electric field
%2- No overlapping between SCP and ECP
%3- Half portion of the bar is considered. This would not
% matter alot since most of the model is based on a per unit
% length parameters.
%4- In case of linear model the ECP resistance is varied in
% order to imitate the voltage dependency since the model is
%linear (Independent of the Voltage)
%%%%%%%%%%%%%%%%%%%%%%%%%%%%%%%%%%%%%%%%%%%%%%%%%%%%%%%%%%%%%%%%%%%%%%%%%%%%
%
%%%%%%%%%%%%%%%%%%%%%%%%%%%%%%%%%%%%%%%%%%%%%%%%%%%%%%%%%%%%%%%%%%%%%%%%%%%%
% Initializing and loading of measurement data
%%%%%%%%%%%%%%%%%%%%%%%%%%%%%%%%%%%%%%%%%%%%%%%%%%%%%%%%%%%%%%%%%%%%%%%%%%%%
clc
clear
%%%%%%%%%%%%%%%%%%%%%%%%%%%%%%%%%%%%%%%%%%%%%%%%%%%%%%%%%%%%%%%%%%%%%%%%%%%%
load('ECPOnlyInput.mat')
% The readings are divided based on the type of coil and
% the study voltage e.g.
```

```
% NonECP_20V is the variable that stores all coil without
% stress grading tape taken at 20V
% ECP_20V is the variable that stores all coil with stress
% grading tape taken at 20V

% The readings are stored in 4 columns matrix where each
% studied f will yield a row of readings i.e.

% [F][C'][C''][Tand]

%%%%%%%%%%%%%%%%%%%%%%%%%%%%%%%%%%%%%%%%%%%%%%%%%%%%%%%%%%%%%%%%%%%%%%%
fmin=0.0001;
fmax=100;
Nf= 20;
Freq = logspace( log10(fmin), log10(fmax), Nf ).';
X=sort(Freq,'descend');
%%%%%%%%%%%%%%%%%%%%%%%%%%%%%%%%%%%%%%%%%%%%%%%%%%%%%%%%%%%%%%%%%%%%%%%
% Parameters setting
%%%%%%%%%%%%%%%%%%%%%%%%%%%%%%%%%%%%%%%%%%%%%%%%%%%%%%%%%%%%%%%%%%%%%%%
%The bar has stright dimensions:
%                   [====][======================][====]
%                     ECP            SCP             ECP
%                   |10cm|<---     120cm     --->||10cm|
% Grading length
grlen = 0.1; %10 cm of ECP
totalbarlength=2*(1.4); %120 cm of SCP
% Model used: sigma(E)= sigma0*exp((nl*E)^(ep))
% sigma0
sigma0=(1.34e-13);
l_c= (2*0.0205+2*0.037);
G0=sigma0*l_c;
% The per unit series resistive element Rs is:
Rs = 1/G0;
% The per unit length lumped elements:
% Series:
Rspu=Rs;
Cspu=0;
% Parallel
% R= U0/(Ipol(10000)) Tested @ 2000V
Rp= (1.4845e+13)*(1/2.8);
Gppu = 1/Rp ;
%%%%%%%%%%%%%%%%%%%%%%%%%%%%%%%%%%%%%%%%%%%%%%%%%%%%%%%%%%%%%%%%%%%%%%%
% Modelling the capacitance of slot exit
%%%%%%%%%%%%%%%%%%%%%%%%%%%%%%%%%%%%%%%%%%%%%%%%%%%%%%%%%%%%%%%%%%%%%%%
% The following part deals with the missing frequency points
% readings and ensure that all data were taken using the same
% set of frequencies (Unify)
NonECP_20 = (interp1(NonECP_20V(:,1),NonECP_20V(:,2)-...
    j*NonECP_20V(:,3),X,'linear','extrap'));
```

```
NonECP_200= (interp1(NonECP_200V(:,1),NonECP_200V(:,2)-...
    j*NonECP_200V(:,3),X,'linear','extrap'));
NonECP_2000= (interp1(NonECP_2000V(:,1),NonECP_2000V(:,2)-...
    j*NonECP_2000V(:,3),X,'linear','extrap'));
NonECP_4000= (interp1(NonECP_4000V(:,1),NonECP_4000V(:,2)-...
    j*NonECP_4000V(:,3),X,'linear','extrap'));
NonECP_6000= (interp1(NonECP_6000V(:,1),NonECP_6000V(:,2)-...
    j*NonECP_6000V(:,3),X,'linear','extrap'));
NonECP_8000= (interp1(NonECP_8000V(:,1),NonECP_8000V(:,2)-...
    j*NonECP_8000V(:,3),X,'linear','extrap'));
NonECP_10000=(interp1(NonECP_10000V(:,1),NonECP_10000V(:,2)...
    -j*NonECP_10000V(:,3),X,'linear','extrap'));
% For Coil without ECP, the data points were averaged
% to ensure that the fit is close to all readings.
cplxydata=((NonECP_20+NonECP_200+NonECP_2000+NonECP_4000...
    +NonECP_6000+NonECP_8000+NonECP_10000)/7);
% Perform lsqcurvefit to find suitble parameters
% to represent the coil insulation.
% Readings could also be used here instead.
%%%%%%%%%%%%%%%%%%%%%%%%%%%%%%%%%%%%%%%%%%%%%%%%%%%%%%%%%%%%%%%%%%%%%%%
ydata2 = [real(cplxydata),imag(-cplxydata)];
x0 = [1 1 1];
lb=[0 0 0];
ub=[7 1 1];
xxx = lsqcurvefit(@cplxreal,x0,X,ydata2,lb,ub)
Cinf = xxx(1)*1e-9
b =xxx(2)*1e-9
n =xxx(3)
% Mica insulation part can be represented by:
yy = Cinf+b*(2*pi*X*1i).^(n-1);
% Per Unit Mica part:
TotalCap_ECPsection=(yy/(totalbarlength));
% Adding stress grading cap
%%%%%%%%%%%%%%%%%%%%%%%%%%%%%%%%%%%%%%%%%%%%%%%%%%%%%%%%%%%%%%%%%%%%%%%
ECPonly_20=(interp1(ECPOnly_20V(:,1),ECPOnly_20V(:,2)...
    -j*ECPOnly_20V(:,3),X,'linear','extrap'))/0.4;
ECPonly_200=(interp1(ECPOnly_200V(:,1),ECPOnly_200V(:,2)...
    -j*ECPOnly_200V(:,3),X,'linear','extrap'))/0.4;

ECPonly_2000=(interp1(ECPOnly_2000V(:,1),ECPOnly_2000V(:,2)...
    -j*ECPOnly_2000V(:,3),X,'linear','extrap'))/0.4;

ECPonly_4000=(interp1(ECPOnly_4000V(:,1),ECPOnly_4000V(:,2)...
    -j*ECPOnly_4000V(:,3),X,'linear','extrap'))/0.4;

ECPonly_6000=(interp1(ECPOnly_6000V(:,1),ECPOnly_6000V(:,2)...
    -j*ECPOnly_6000V(:,3),X,'linear','extrap'))/0.4;

ECPonly_8000=(interp1(ECPOnly_8000V(:,1),ECPOnly_8000V(:,2)...
```

```
    -j*ECPOnly_8000V(:,3),X,'linear','extrap'))/0.4;

ECPonly_10000=(interp1(ECPOnly_10000V(:,1),...
    ECPOnly_10000V(:,2)-j*ECPOnly_10000V(:,3),...
    X,'linear','extrap'))/0.4;
% Adding Mica+SiC tape capacitance
TotalCapUnderECP(:,1)=...
    (TotalCap_ECPsection)+(ECPonly_200/2)*1e-9;
TotalCapUnderECP(:,2)=...
    (TotalCap_ECPsection)+(ECPonly_2000/2)*1e-9;
TotalCapUnderECP(:,3)=...
    (TotalCap_ECPsection)+(ECPonly_6000/2)*1e-9;
TotalCapUnderECP(:,4)=...
    (TotalCap_ECPsection)+(ECPonly_10000/2)*1e-9;
Cppu =TotalCapUnderECP(:,1);
Cend=0;
% Load the variables that has all the measured data
F = X;
%%%%%%%%%%%%%%%%%%%%%%%%%%%%%%%%%%%%%%%%%%%%%%%%%%%%%%%%%%%%%%%%%%%%%%%
% Calculation of the complex capacitance for 100% Rs
%%%%%%%%%%%%%%%%%%%%%%%%%%%%%%%%%%%%%%%%%%%%%%%%%%%%%%%%%%%%%%%%%%%%%%%
% These calculations are based on Eq. 41-44 on page 24
Zspu_lc = 1./( 1/(Rspu) + 1j.*2*pi.*F.*Cspu );
Yppu_lc = 1i.*2.*pi.*F.*Cppu + Gppu;
Zo = sqrt( Zspu_lc ./ Yppu_lc );
propcon = sqrt( Yppu_lc .* Zspu_lc );
Zi = Zo ./ ( tanh(propcon*grlen) );
C_end_r1 = 1 ./ ( 1j.*2*pi.*F.*Zi );
%%%%%%%%%%%%%%%%%%%%%%%%%%%%%%%%%%%%%%%%%%%%%%%%%%%%%%%%%%%%%%%%%%%%%%%
% Calculation of the complex capacitance for 10% Rs
%%%%%%%%%%%%%%%%%%%%%%%%%%%%%%%%%%%%%%%%%%%%%%%%%%%%%%%%%%%%%%%%%%%%%%%
% These calculations are based on Eq. 41-44 on page 24
Zspu_lc = 1./( 1/(Rspu*0.1) + j*2*pi*F*Cspu );
Yppu_lc = 1j.*2.*pi.*F.*Cppu + Gppu;
Zo = sqrt( Zspu_lc ./ Yppu_lc );
propcon = sqrt( Yppu_lc .* Zspu_lc );
Zi = Zo ./ ( tanh(propcon*grlen) );
C_end_r01 = 1 ./ ( j.*2*pi.*F.*Zi );
%%%%%%%%%%%%%%%%%%%%%%%%%%%%%%%%%%%%%%%%%%%%%%%%%%%%%%%%%%%%%%%%%%%%%%%
% Calculation of the complex capacitance for 10% Rs
%%%%%%%%%%%%%%%%%%%%%%%%%%%%%%%%%%%%%%%%%%%%%%%%%%%%%%%%%%%%%%%%%%%%%%%
% These calculations are based on Eq. 41-44 on page 24
Zspu_lc = 1./( 1/(Rspu*0.01) + j*2*pi*F*Cspu );
Yppu_lc = j.*2.*pi.*F.*Cppu + Gppu;
Zo = sqrt( Zspu_lc ./ Yppu_lc );
propcon = sqrt( Yppu_lc .* Zspu_lc );
Zi = Zo ./ ( tanh(propcon*grlen) );
C_end_r001 = 1 ./ ( j.*2.*pi.*F.*Zi );
%%%%%%%%%%%%%%%%%%%%%%%%%%%%%%%%%%%%%%%%%%%%%%%%%%%%%%%%%%%%%%%%%%%%%%%
```

```
%%%%%%%%%%%%%%%%%%%%%%%%%%%%%%%%%%%%%%%%%%%%%%%%%%%%%%%%%%%%%%%%%%%%%%%
% Plots
%%%%%%%%%%%%%%%%%%%%%%%%%%%%%%%%%%%%%%%%%%%%%%%%%%%%%%%%%%%%%%%%%%%%%%%
k_scaling = 1.4;
width = (17.6) * k_scaling;
hight = 8.8* k_scaling;
figurespec
cmap = colormap(jet(7))/1.1;
cmap3 = colormap(jet(7))/1.1;
figure(8)
subplot(1,2,1);
loglog(ECPOnly_200V(:,1),ECPOnly_200V(:,2),'-bo','color' ...
    ,'k','MarkerFaceColor',cmap3(2,:),...
    'MarkerEdgeColor','k','linewidth',1)
hold on
loglog(ECPOnly_2000V(:,1),ECPOnly_2000V(:,2),'-bo'...
    ,'color','k','MarkerFaceColor',cmap3(3,:)...
    ,'MarkerEdgeColor','k','linewidth',1)
hold on
loglog(ECPOnly_6000V(:,1),ECPOnly_6000V(:,2),...
    '-bo','color','k','MarkerFaceColor',cmap3(5,:)...
    ,'MarkerEdgeColor','k','linewidth',1)
hold on
loglog(ECPOnly_10000V(:,1),ECPOnly_10000V(:,2),'-bo',...
    'color','k','MarkerFaceColor',cmap3(7,:),...
    'MarkerEdgeColor','k','linewidth',1)
hold on
loglog(F,real(C_end_r1)*2e9,'->','MarkerFaceColor'...
    ,'w','color','k','MarkerEdgeColor','k','LineWidth',1)
hold on
loglog(F,real(C_end_r01)*2e9,'->','MarkerFaceColor'...
    ,'w','color','k','MarkerEdgeColor','k','LineWidth',1)
hold on
loglog(F,real(C_end_r001)*2e9,'->','MarkerFaceColor'...
    ,'w','color','k','MarkerEdgeColor','k','LineWidth',1)

h = text(150,(real(C_end_r001(1)))*2e9,'0.01R_0'...
    ,'Rotation',-45);
h1 = text(150,(real(C_end_r01(1)))*2e9,'0.1R_0'...
    ,'Rotation',-45);
h2 = text(150,(real(C_end_r1(1)))*2e9,'R_0'...
    ,'Rotation',-45);
xlim([1e-5 1e3])
ylim([1e-4 1.1])

title('Linear model of the end section')

xlabel('Frequency [Hz]')
ylabel('C'' [nF]')
```

```
l1 = plot([NaN,NaN],'s','MarkerFaceColor',cmap3(2,:),...
    'MarkerEdgeColor',cmap3(2,:),'linewidth',2);
l2 = plot([NaN,NaN],'s','MarkerFaceColor',cmap3(3,:),...
    'MarkerEdgeColor',cmap3(3,:),'linewidth',2);
l3 = plot([NaN,NaN],'s','MarkerFaceColor',cmap3(5,:),...
    'MarkerEdgeColor',cmap3(5,:),'linewidth',2);
l4 = plot([NaN,NaN],'s','MarkerFaceColor',cmap3(7,:),...
    'MarkerEdgeColor',cmap3(7,:),'linewidth',2);
l5 = plot([NaN,NaN],'-bo','MarkerFaceColor','w','color'...
    ,'k','MarkerEdgeColor','k','linewidth',1);
l7 = plot([NaN,NaN],'->','MarkerFaceColor','w','color'...
    ,'k','MarkerEdgeColor','k','linewidth',1);
leg1=legend([l1, l2, l3,l4, l5,l7], {'200 V','2000 V'...
    ,'6000 V','10000 V','Measurements','Linear Model'}...
    ,'location','southwest');

subplot(1,2,2);
loglog(ECPOnly_200V(:,1),ECPOnly_200V(:,3),'-bo',...
    'color','k','MarkerFaceColor',cmap3(2,:),...
    'MarkerEdgeColor','k','linewidth',1)
hold on
loglog(ECPOnly_2000V(:,1),ECPOnly_2000V(:,3),...
    '-bo','color','k','MarkerFaceColor',cmap3(3,:)...
    ,'MarkerEdgeColor','k','linewidth',1)
hold on
loglog(ECPOnly_6000V(:,1),ECPOnly_6000V(:,3),'-bo'...
    ,'color','k','MarkerFaceColor',cmap3(5,:),...
    'MarkerEdgeColor','k','linewidth',1)
hold on

loglog(ECPOnly_10000V(:,1),ECPOnly_10000V(:,3),'-bo',...
    'color','k','MarkerFaceColor',cmap3(7,:),...
    'MarkerEdgeColor','k','linewidth',1)
hold on
loglog(F,imag(-C_end_r1)*2e9,'->','MarkerFaceColor',...
    'w','color','k','MarkerEdgeColor','k','LineWidth',1)
hold on
loglog(F,imag(-C_end_r01)*2e9,'->','MarkerFaceColor',...
    'w','color','k','MarkerEdgeColor','k','LineWidth',1)
hold on
loglog(F,imag(-C_end_r001)*2e9,'->','MarkerFaceColor',...
    'w','color','k','MarkerEdgeColor','k','LineWidth',1)

h = text(150,(imag(-C_end_r001(1)))*2e9,'0.01R_0',...
    'Rotation',-45);
h1 = text(150,(imag(-C_end_r01(1)))*2e9,'0.1R_0',...
    'Rotation',-45);
h2 = text(150,(imag(-C_end_r1(1)))*2e9,'R_0',...
```

```
    'Rotation',-45);
xlim([1e-5 1e3])
ylim([1e-4 0.5])
l1 = plot([NaN,NaN],'s','MarkerFaceColor',...
    cmap3(2,:),'MarkerEdgeColor',cmap3(2,:),'linewidth',2);
l2 = plot([NaN,NaN],'s','MarkerFaceColor',...
    cmap3(3,:),'MarkerEdgeColor',cmap3(3,:),'linewidth',2);
l3 = plot([NaN,NaN],'s','MarkerFaceColor',...
    cmap3(5,:),'MarkerEdgeColor',cmap3(5,:),'linewidth',2);
l4 = plot([NaN,NaN],'s','MarkerFaceColor',...
    cmap3(7,:),'MarkerEdgeColor',cmap3(7,:),'linewidth',2);

l5 = plot([NaN,NaN],'-bo','MarkerFaceColor','w',...
    'color','k','MarkerEdgeColor','k','linewidth',1);
l6 = plot([NaN,NaN],'-s','MarkerFaceColor','w',...
    'color','k','MarkerEdgeColor','k','linewidth',1);
l7 = plot([NaN,NaN],'->','MarkerFaceColor','w',...
    'color','k','MarkerEdgeColor','k','linewidth',1);
leg1=legend([l1, l2, l3,l4, l5,l7], {'200 V',...
    '2000 V','6000 V','10000 V','Measurements',...
    'Linear Model'},'location','southwest');

title('Linear model of the end section')
xlabel('Frequency [Hz]')
ylabel('C'''' [nF]')
%%%%%%%%%%%%%%%%%%%%%%%%%%%%%%%%%%%%%%%%%%%%%%%%%%%%%%%%%%%%%%%%%%%%%%%
%END
%%%%%%%%%%%%%%%%%%%%%%%%%%%%%%%%%%%%%%%%%%%%%%%%%%%%%%%%%%%%%%%%%%%%%%%
```

B. Nonlinear distributed-element model Matlab Code

```
%%%%%%%%%%%%%%%%%%%%%%%%%%%%%%%%%%%%%%%%%%%%%%%%%%%%%%%%%%%%%%%%%%%%%%%%
% Slot End Section NonLinear Model
%%%%%%%%%%%%%%%%%%%%%%%%%%%%%%%%%%%%%%%%%%%%%%%%%%%%%%%%%%%%%%%%%%%%%%%%
% By Amar Abideen - June 2020
%%%%%%%%%%%%%%%%%%%%%%%%%%%%%%%%%%%%%%%%%%%%%%%%%%%%%%%%%%%%%%%%%%%%%%%%
% Credit: This code was rewritten based on Nathaniel Taylor
% previous code during his PhD work
%%%%%%%%%%%%%%%%%%%%%%%%%%%%%%%%%%%%%%%%%%%%%%%%%%%%%%%%%%%%%%%%%%%%%%%%
% This Code was written to implement the nummerical model
% of a stator coil sample
%%%%%%%%%%%%%%%%%%%%%%%%%%%%%%%%%%%%%%%%%%%%%%%%%%%%%%%%%%%%%%%%%%%%%%%%
%%%%%%%%%%%%%%%%%%%%%%%%%%%%%%%%%%%%%%%%%%%%%%%%%%%%%%%%%%%%%%%%%%%%%%%%
% Note:
%%%%%%%%%%%%%%%%%%%%%%%%%%%%%%%%%%%%%%%%%%%%%%%%%%%%%%%%%%%%%%%%%%%%%%%%
% The assumptions made:
%1- No overlapping between SCP and ECP
%3- Half portion of the bar is considered. This would not
% matter alot since most of the model is based on a per unit
% length parameters.
%%%%%%%%%%%%%%%%%%%%%%%%%%%%%%%%%%%%%%%%%%%%%%%%%%%%%%%%%%%%%%%%%%%%%%%%
%
%%%%%%%%%%%%%%%%%%%%%%%%%%%%%%%%%%%%%%%%%%%%%%%%%%%%%%%%%%%%%%%%%%%%%%%%
% Initializing and loading of measurement data
%%%%%%%%%%%%%%%%%%%%%%%%%%%%%%%%%%%%%%%%%%%%%%%%%%%%%%%%%%%%%%%%%%%%%%%%
clc
clear
%%%%%%%%%%%%%%%%%%%%%%%%%%%%%%%%%%%%%%%%%%%%%%%%%%%%%%%%%%%%%%%%%%%%%%%%
load('ECPOnlyInput.mat')
% The readings are divided based on the type of coil and
% the study voltage e.g.

% NonECP_20V is the variable that stores all coil without
% stress grading tape taken at 20V
% ECP_20V is the variable that stores all coil with stress
% grading tape taken at 20V

% The readings are stored in 4 columns matrix where each
% studied f will yield a row of readings i.e.

% [F][C'][C''][Tand]

%%%%%%%%%%%%%%%%%%%%%%%%%%%%%%%%%%%%%%%%%%%%%%%%%%%%%%%%%%%%%%%%%%%%%%%%
fmin=0.0001;
fmax=100;
Nf= 20;
Freq = logspace( log10(fmin), log10(fmax), Nf ).';
X=sort(Freq,'descend');
```

```
%%%%%%%%%%%%%%%%%%%%%%%%%%%%%%%%%%%%%%%%%%%%%%%%%%%%%%%%%%%%%%%%%%%%%%%%%%%%
% Parameters setting
%%%%%%%%%%%%%%%%%%%%%%%%%%%%%%%%%%%%%%%%%%%%%%%%%%%%%%%%%%%%%%%%%%%%%%%%%%%%
%The bar has stright dimensions:
%                   [====][======================][====]
%                     ECP            SCP             ECP
%                   |10cm|<---     120cm     --->||10cm|
% Grading length
grlen = 0.1; %10 cm of ECP
totalbarlength=2*(1.4);
% Model used: sigma(E)= sigma0*exp((nl*E)^(ep))
% sigma0
sigma0=(1.34e-13);
l_c= (2*0.0205+2*0.037);
G0=sigma0*l_c;
nl = (1/16070)^0.66;
ep = 0.66;
% The per unit series resistive element Rs is:
Rs = 1/G0;
% The per unit length lumped elements:
% Series:
Rspu=Rs;
Cspu=0;
% Parallel
% R= U0/(Ipol(10000)) Tested @ 2000V
Rp= (1.4845e+13)*(1/2.8);
Gppu = 1/Rp ;
%%%%%%%%%%%%%%%%%%%%%%%%%%%%%%%%%%%%%%%%%%%%%%%%%%%%%%%%%%%%%%%%%%%%%%%%%%%%
% Modelling the capacitance of slot exit
%%%%%%%%%%%%%%%%%%%%%%%%%%%%%%%%%%%%%%%%%%%%%%%%%%%%%%%%%%%%%%%%%%%%%%%%%%%%
% The following part deals with the missing frequency points
% readings and ensure that all data were taken using the same
% set of frequencies (Unify)
NonECP_20 = (interp1(NonECP_20V(:,1),NonECP_20V(:,2)-...
    j*NonECP_20V(:,3),X,'linear','extrap'));
NonECP_200= (interp1(NonECP_200V(:,1),NonECP_200V(:,2)-...
    j*NonECP_200V(:,3),X,'linear','extrap'));
NonECP_2000= (interp1(NonECP_2000V(:,1),NonECP_2000V(:,2)-...
    j*NonECP_2000V(:,3),X,'linear','extrap'));
NonECP_4000= (interp1(NonECP_4000V(:,1),NonECP_4000V(:,2)-...
    j*NonECP_4000V(:,3),X,'linear','extrap'));
NonECP_6000= (interp1(NonECP_6000V(:,1),NonECP_6000V(:,2)-...
    j*NonECP_6000V(:,3),X,'linear','extrap'));
NonECP_8000= (interp1(NonECP_8000V(:,1),NonECP_8000V(:,2)-...
    j*NonECP_8000V(:,3),X,'linear','extrap'));
NonECP_10000=(interp1(NonECP_10000V(:,1),NonECP_10000V(:,2)...
    -j*NonECP_10000V(:,3),X,'linear','extrap'));
% For Coil without ECP, the data points were averaged
% to ensure that the fit is close to all readings.
```

```
cplxydata=((NonECP_20+NonECP_200+NonECP_2000+NonECP_4000...
    +NonECP_6000+NonECP_8000+NonECP_10000)/7);
% Perform lsqcurvefit to find suitble parameters
% to represent the coil insulation.
% Readings could also be used here instead.
%%%%%%%%%%%%%%%%%%%%%%%%%%%%%%%%%%%%%%%%%%%%%%%%%%%%%%%%%%%%%%%%%%%%%%%
ydata2 = [real(cplxydata),imag(-cplxydata)];
x0 = [1 1 1];
lb=[0 0 0];
ub=[7 1 1];
xxx = lsqcurvefit(@cplxreal,x0,X,ydata2,lb,ub) ;
Cinf = xxx(1)*1e-9;
b =xxx(2)*1e-9;
n =xxx(3);
% Mica insulation part can be represented by:
yy = Cinf+b*(2*pi*X*1i).^(n-1);
% Per Unit Mica part:
TotalCap_ECPsection=(yy/(totalbarlength));
% Adding stress grading cap
%%%%%%%%%%%%%%%%%%%%%%%%%%%%%%%%%%%%%%%%%%%%%%%%%%%%%%%%%%%%%%%%%%%%%%%
ECPonly_20=(interp1(ECPOnly_20V(:,1),ECPOnly_20V(:,2)...
    -j*ECPOnly_20V(:,3),X,'linear','extrap'))/0.4;
ECPonly_200=(interp1(ECPOnly_200V(:,1),ECPOnly_200V(:,2)...
    -j*ECPOnly_200V(:,3),X,'linear','extrap'))/0.4;

ECPonly_2000=(interp1(ECPOnly_2000V(:,1),ECPOnly_2000V(:,2)...
    -j*ECPOnly_2000V(:,3),X,'linear','extrap'))/0.4;

ECPonly_4000=(interp1(ECPOnly_4000V(:,1),ECPOnly_4000V(:,2)...
    -j*ECPOnly_4000V(:,3),X,'linear','extrap'))/0.4;

ECPonly_6000=(interp1(ECPOnly_6000V(:,1),ECPOnly_6000V(:,2)...
    -j*ECPOnly_6000V(:,3),X,'linear','extrap'))/0.4;

ECPonly_8000=(interp1(ECPOnly_8000V(:,1),ECPOnly_8000V(:,2)...
    -j*ECPOnly_8000V(:,3),X,'linear','extrap'))/0.4;

ECPonly_10000=(interp1(ECPOnly_10000V(:,1),...
    ECPOnly_10000V(:,2)-j*ECPOnly_10000V(:,3),...
    X,'linear','extrap'))/0.4;
% Adding Mica+SiC tape capacitance
TotalCapUnderECP(:,1)=...
    (TotalCap_ECPsection)+(ECPonly_200/2)*1e-9;
TotalCapUnderECP(:,2)=...
    (TotalCap_ECPsection)+(ECPonly_2000/2)*1e-9;
TotalCapUnderECP(:,3)=...
    (TotalCap_ECPsection)+(ECPonly_6000/2)*1e-9;
TotalCapUnderECP(:,4)=...
    (TotalCap_ECPsection)+(ECPonly_10000/2)*1e-9;
```

```
Cppu =TotalCapUnderECP(:,1);
Cend=0.01*totalbarlength*yy(1);
%%%%%%%%%%%%%%%%%%%%%%%%%%%%%%%%%%%%%%%%%%%%%%%%%%%%%%%%%%%%%%%%%%%%%%%%%%%%
V = [200 2000 6000 10000]; % Peak Voltage
phi = 0;  % Phase shift
% Nf: Number of studied frequency points
Nf = 20;
fmin=0.0001;
fmax=100;
Freq = logspace( log10(fmin), log10(fmax), Nf ).';
% Nv: Number of studied Peak voltage points
Nv = length(V);
% Nh: Number of harmonics considered
Nh = 9;
% Ncyc: Number of cycles considered
Ncyc = 2;
% Nskip: Number of cycles to skip (To skip transients)
Nskip = 4;
% Nppc: Number of sample points
Nppc = 32;
% Nt: Number of time points
Nt = Ncyc * Nppc;
% Nseg: Number of mesh points
Nx = 32;
%%%%%%%%%%%%%%%%%%%%%%%%%%%%%%%%%%%%%%%%%%%%%%%%%%%%%%%%%%%%%%%%%%%%%%%%%%%%
% Solver Settings
odesolver = @ode113;
reltol = 1e-4;  % default: 1e-3
abstol = 1e-6;  % default: 1e-6
maxstep_relTs = 1/2;
%%%%%%%%%%%%%%%%%%%%%%%%%%%%%%%%%%%%%%%%%%%%%%%%%%%%%%%%%%%%%%%%%%%%%%%%%%%%
% Initialize data storage

% Time-domain (from ODE solution): 3D array, time along 3rd
%dimension,voltage amplitude and frequency along 1st and 2nd.


volt_time = NaN*zeros( Nv, Nf, Nt );
curr_time = volt_time;
times = volt_time;

%%%%%%%%%%%%%%%%%%%%%%%%%%%%%%%%%%%%%%%%%%%%%%%%%%%%%%%%%%%%%%%%%%%%%%%%%%%%

% Frequency-domain (from FFT on time-domain):
% similar, but 3rd dimension is harmonic order.
% Correct points from raw FFT output have been
% selected and scaled so that this output is the integer
% harmonics regardless of how many cycles were used, and is
% scaled so a sine in time gets the same magnitude in
```

```
% this output.

volt_freq = NaN*zeros( Nv, Nf, Nh );
curr_freq = volt_freq;
freq_freq = volt_freq;

%%%%%%%%%%%%%%%%%%%%%%%%%%%%%%%%%%%%%%%%%%%%%%%%%%%%%%%%%%%%%%%%%%%%%%%

global vp w
for vidx=1:Nv,
    Ur_pervious=0;
    for fidx=1:Nf,
       % Adjust Cp based on studied frequency and voltage
       Cp =TotalCapUnderECP(fidx,vidx);
       Cppu = Cp ;
       % Set the sinusoid parameters
        f = F(fidx);
        w = 2*pi*f;
        vp = V(vidx);
%%%%%%%%%%%%%%%%%%%%%%%%%%%%%%%%%%%%%%%%%%%%%%%%%%%%%%%%%%%%%%%%%%%%%%%

        Tc = 1/f; % Period of fundemental freqency
        Ts = Tc/Nppc; % Sampling period
        maxstep = maxstep_relTs * Ts;

%%%%%%%%%%%%%%%%%%%%%%%%%%%%%%%%%%%%%%%%%%%%%%%%%%%%%%%%%%%%%%%%%%%%%%%

        % Set the PDE solver
        %
        options = ...
        odeset( 'MaxStep', maxstep, 'RelTol', ...
        reltol,'AbsTol', abstol);

        % Initialize space vector
        x = linspace( 0, grlen, Nx );
        % Initialize time vector
        t_all = ((-Nskip*Nppc):(Nt-1)) * Ts;

%%%%%%%%%%%%%%%%%%%%%%%%%%%%%%%%%%%%%%%%%%%%%%%%%%%%%%%%%%%%%%%%%%%%%%%

        % pdepe solves a 1-D parabolic and elliptic PDE
        %
        %  The standard form:
        %  c * du/dt  = x^-m * d/dx ( x^m * f ) + s;
        %
        %  where c, f and s are f(x,t,u,du/dt)
        %
        % Boundary and initial conditions are written in a
        % a way similar to the example shown in:
```

```
        % https://se.mathworks.com/help/matlab/ref/pdepe.html


        soln_all = pdepe( 0, @nlc_pde, @nlc_ic,...
            @nlc_bc, x, t_all, options );

        % Set a scope on the data after two cycles(Nskip)
        % and include the number of (Nppc) points

        t = t_all( (Nskip*Nppc+1):end );
        soln = soln_all( (Nskip*Nppc+1):end, : );

        u0 = zeros( Nt, 1 );
        du0dt = zeros( Nt, 1 );

        % Now, interpolate the PDE solution to find values
        % thats corresponds with our time scope
        for tidx=1:Nt,
            [ u0(tidx), du0dt(tidx) ] = pdeval( 0, x,...
                soln(tidx,:), x(1) );
        end
        % first element's potential is the supply voltage
        vs = u0;
        % first element's flow is (minus)the supply current
        i  =  -du0dt .* 1/Rspu .* exp( nl * abs(-du0dt).^ep );

    %%%%%%%%%%%%%%%%%%%%%%%%%%%%%%%%%%%%%%%%%%%%%%%%%%%%%%%%%%%%%%%%
     % Record the obtained time domain data in the 3D storage
        times( vidx, fidx, : ) = t;
        volt_time( vidx, fidx, : ) = vs;
        curr_time( vidx, fidx, : ) = i;
        pdesolns{ vidx, fidx } = soln;

        % Preform fast fourier transformation to transfer
        % data to frequency domain

        fft_i = fft( i );
        curr_freq( vidx, fidx, : ) = 2/length(i) *...
            fft_i( 1 + (1:Nh)*Ncyc );

        i_dc = fft_i(1)/length(i);


        fft_vs = fft( vs );
        volt_freq( vidx, fidx, : ) = 2/length(vs) *...
            fft_vs( 1 + (1:Nh)*Ncyc );
        vs_dc = fft_vs(1)/length(i);

        % frequency, including harmonics
```

```
        freq_freq( vidx, fidx, : ) = f * (1:Nh);


    end
end
%%%%%%%%%%%%%%%%%%%%%%%%%%%%%%%%%%%%%%%%%%%%%%%%%%%%%%%%%%%%%%%%%%%%%%%
% Calculate the complex capacitance based on
% C(w)=I/(w*U)
Ccomp = squeeze( curr_freq(:,:,1) ./...
    ( 2*pi*j*freq_freq(:,:,1) .* volt_freq(:,:,1) ) );
y=2*Ccomp;
load('ECPOnlyInput.mat')
Fx=sort(Freq,'descend')';
%%%%%%%%%%%%%%%%%%%%%%%%%%%%%%%%%%%%%%%%%%%%%%%%%%%%%%%%%%%%%%%%%%%%%%%
% Plots
%%%%%%%%%%%%%%%%%%%%%%%%%%%%%%%%%%%%%%%%%%%%%%%%%%%%%%%%%%%%%%%%%%%%%%%
k_scaling = 1.4;
width = (17.6) * k_scaling;
hight = 8.8* k_scaling;
figurespec
cmap = colormap(jet(7))/1.1;
cmap3 = colormap(jet(7))/1.1;
figure(8)
subplot(1,2,1);

loglog(ECPOnly_200V(:,1),ECPOnly_200V(:,2),'-bo','color' ...
    ,'k','MarkerFaceColor',cmap3(2,:),...
    'MarkerEdgeColor','k','linewidth',1)
hold on
loglog(ECPOnly_2000V(:,1),ECPOnly_2000V(:,2),'-bo'...
    ,'color','k','MarkerFaceColor',cmap3(3,:)...
    ,'MarkerEdgeColor','k','linewidth',1)
hold on
loglog(ECPOnly_6000V(:,1),ECPOnly_6000V(:,2),...
    '-bo','color','k','MarkerFaceColor',cmap3(5,:)...
    ,'MarkerEdgeColor','k','linewidth',1)
hold on
loglog(ECPOnly_10000V(:,1),ECPOnly_10000V(:,2),'-bo',...
    'color','k','MarkerFaceColor',cmap3(7,:),...
    'MarkerEdgeColor','k','linewidth',1)
hold on

loglog(Fx,real(y(1,:))*1e9,'-sq','MarkerFaceColor'...
    ,cmap3(2,:),'color','k','MarkerEdgeColor','k',...
    'LineWidth',1)
hold on
loglog(Fx,real(y(2,:))*1e9,'-sq','MarkerFaceColor'...
    ,cmap3(3,:),'color','k','MarkerEdgeColor','k',...
    'LineWidth',1)
```

```
hold on
loglog(Fx,real(y(3,:))*1e9,'-sq','MarkerFaceColor'...
    ,cmap3(5,:),'color','k','MarkerEdgeColor','k',...
    'LineWidth',1)
hold on
loglog(Fx,real(y(4,:))*1e9,'-sq','MarkerFaceColor'...
    ,cmap3(7,:),'color','k','MarkerEdgeColor','k',...
    'LineWidth',1)
xlim([1e-5 1e3])
ylim([1e-4 1.1])

title('Nonlinear model of the end section')

xlabel('Frequency [Hz]')
ylabel('C'' [nF]')

l1 = plot([NaN,NaN],'s','MarkerFaceColor',cmap3(2,:),...
    'MarkerEdgeColor',cmap3(2,:),'linewidth',2);
l2 = plot([NaN,NaN],'s','MarkerFaceColor',cmap3(3,:),...
    'MarkerEdgeColor',cmap3(3,:),'linewidth',2);
l3 = plot([NaN,NaN],'s','MarkerFaceColor',cmap3(5,:),...
    'MarkerEdgeColor',cmap3(5,:),'linewidth',2);
l4 = plot([NaN,NaN],'s','MarkerFaceColor',cmap3(7,:),...
    'MarkerEdgeColor',cmap3(7,:),'linewidth',2);
l5 = plot([NaN,NaN],'-bo','MarkerFaceColor','w','color'...
    ,'k','MarkerEdgeColor','k','linewidth',1);
l7 = plot([NaN,NaN],'-sq','MarkerFaceColor','w','color'...
    ,'k','MarkerEdgeColor','k','linewidth',1);
leg1=legend([l1, l2, l3,l4, l5,l7], {'200 V','2000 V'...
    ,'6000 V','10000 V','Measurements','Linear Model'}...
    ,'location','southwest');

subplot(1,2,2);
loglog(ECPOnly_200V(:,1),ECPOnly_200V(:,3),'-bo',...
    'color','k','MarkerFaceColor',cmap3(2,:),...
    'MarkerEdgeColor','k','linewidth',1)
hold on
loglog(ECPOnly_2000V(:,1),ECPOnly_2000V(:,3),...
    '-bo','color','k','MarkerFaceColor',cmap3(3,:)...
    ,'MarkerEdgeColor','k','linewidth',1)
hold on
loglog(ECPOnly_6000V(:,1),ECPOnly_6000V(:,3),'-bo'...
    ,'color','k','MarkerFaceColor',cmap3(5,:),...
    'MarkerEdgeColor','k','linewidth',1)
hold on

loglog(ECPOnly_10000V(:,1),ECPOnly_10000V(:,3),'-bo',...
    'color','k','MarkerFaceColor',cmap3(7,:),...
    'MarkerEdgeColor','k','linewidth',1)
```

```
hold on

loglog(Fx,-imag(y(1,:))*1e9,'-sq','MarkerFaceColor'...
    ,cmap3(2,:),'color','k','MarkerEdgeColor','k',...
    'LineWidth',1)
hold on
loglog(Fx,-imag(y(2,:))*1e9,'-sq','MarkerFaceColor'...
    ,cmap3(3,:),'color','k','MarkerEdgeColor','k',...
    'LineWidth',1)
hold on
loglog(Fx,-imag(y(3,:))*1e9,'-sq','MarkerFaceColor'...
    ,cmap3(5,:),'color','k','MarkerEdgeColor','k',...
    'LineWidth',1)
hold on
loglog(Fx,-imag(y(4,:))*1e9,'-sq','MarkerFaceColor'...
    ,cmap3(7,:),'color','k','MarkerEdgeColor','k',...
    'LineWidth',1)
xlim([1e-5 1e3])
ylim([1e-4 0.5])
l1 = plot([NaN,NaN],'s','MarkerFaceColor',...
    cmap3(2,:),'MarkerEdgeColor',cmap3(2,:),'linewidth',2);
l2 = plot([NaN,NaN],'s','MarkerFaceColor',...
    cmap3(3,:),'MarkerEdgeColor',cmap3(3,:),'linewidth',2);
l3 = plot([NaN,NaN],'s','MarkerFaceColor',...
    cmap3(5,:),'MarkerEdgeColor',cmap3(5,:),'linewidth',2);
l4 = plot([NaN,NaN],'s','MarkerFaceColor',...
    cmap3(7,:),'MarkerEdgeColor',cmap3(7,:),'linewidth',2);

l5 = plot([NaN,NaN],'-bo','MarkerFaceColor','w',...
    'color','k','MarkerEdgeColor','k','linewidth',1);
l6 = plot([NaN,NaN],'-s','MarkerFaceColor','w',...
    'color','k','MarkerEdgeColor','k','linewidth',1);
l7 = plot([NaN,NaN],'-sq','MarkerFaceColor','w',...
    'color','k','MarkerEdgeColor','k','linewidth',1);
leg1=legend([l1, l2, l3,l4, l5,l7], {'200 V',...
    '2000 V','6000 V','10000 V','Measurements',...
    'Nonlinear Model'},'location','southwest');

title('Nonlinear model of the end section')
xlabel('Frequency [Hz]')
ylabel('C'''' [nF]')
%%%%%%%%%%%%%%%%%%%%%%%%%%%%%%%%%%%%%%%%%%%%%%%%%%%%%%%%%%%%%%%%
%END
%%%%%%%%%%%%%%%%%%%%%%%%%%%%%%%%%%%%%%%%%%%%%%%%%%%%%%%%%%%%%%%%

%%%%%%%%%%%%%%%%%%%%%%%%%%%%%%%%%%%%%%%%%%%%%%%%%%%%%%%%%%%%%%%%
function [ c, f, s ] = nlc_pde( x, t, u, dudx )
global Rspu Cppu Gppu Cspu nl ep grlen
c = Cppu;
```

```
f = nl_iv_relation( dudx );
s = u*Gppu;
% c * du/dt  = x^-m * d/dx ( x^m * f ) + s;
end
%%%%%%%%%%%%%%%%%%%%%%%%%%%%%%%%%%%%%%%%%%%%%%%%%%%%%%%%%%%%%%%%%%%%%%%%%%%%
function u0 = nlc_ic(x);

% for the moment, have initial-conditions all zero
% (better way? linear final soln for given V and f?)
u0 = 0*x;

end
%%%%%%%%%%%%%%%%%%%%%%%%%%%%%%%%%%%%%%%%%%%%%%%%%%%%%%%%%%%%%%%%%%%%%%%%%%%%
function [ pl, ql, pr, qr ] = nlc_bc( xl, ul, xr, ur, t )
global Gend
% left:  essential BC
pl = ul - v_supply(t);
ql = 0;
% right: mixed BC
pr = Gend*ur ;
qr = 1;

end
%%%%%%%%%%%%%%%%%%%%%%%%%%%%%%%%%%%%%%%%%%%%%%%%%%%%%%%%%%%%%%%%%%%%%%%%%%%%
function vs = v_supply( t )


global vp w phi
vs = vp * sin( w*t + phi );

end
%%%%%%%%%%%%%%%%%%%%%%%%%%%%%%%%%%%%%%%%%%%%%%%%%%%%%%%%%%%%%%%%%%%%%%%%%%%%

function I = nl_iv_relation( E )

global  Rspu nl ep

% the non-linear SiC grading equation used here
I =  E .* 1/Rspu .* exp( nl * abs(E).^ep );
end
%%%%%%%%%%%%%%%%%%%%%%%%%%%%%%%%%%%%%%%%%%%%%%%%%%%%%%%%%%%%%%%%%%%%%%%%%%%%
```

TRITA TRITA-EECS-EX-2020:548